Mon. Not. R. Astron. Soc. **390,** 93–117 (2008) doi:10.1111/j.1365-2966.2008.13712.x

The SAURON project – XII. Kinematic substructures in early-type galaxies: evidence for discs in fast rotators

Davor Krajnović,[1⋆] R. Bacon,[2] Michele Cappellari,[1] Roger L. Davies,[1] P. T. de Zeeuw,[3,4] Eric Emsellem,[2] Jesús Falcón-Barroso,[5] Harald Kuntschner,[6] Richard M. McDermid,[7] Reynier F. Peletier,[8] Marc Sarzi,[9] Remco C. E. van den Bosch[4] and Glenn van de Ven[10]†

[1]*Denys Wilkinson Building, University of Oxford, Keble Road, Oxford OX1 3RH*
[2]*Université de Lyon, France; Université Lyon 1, F-69007; CRAL, Observatoire de Lyon, F-69230 Saint Genis Laval; CNRS, UMR 5574; ENS de Lyon, France*
[3]*European Southern Observatory, Karl-Schwarzschild-Str 2, 85748 Garching, Germany*
[4]*Sterrewacht Leiden, Leiden University, Niels Bohrweg 2, 2333 CA Leiden, the Netherlands*
[5]*European Space and Technology Centre (ESTEC), Keplerlaan 1, Postbus 299, 2200 AG Noordwijk, the Netherlands*
[6]*Space Telescope European Coordinating Facility, European Southern Observatory, Karl-Schwarzschild-Str 2, 85748 Garching, Germany*
[7]*Gemini Observatory, Northern Operations Centre, 670 N. A'ohoku Place, Hilo, Hawaii 96720, USA*
[8]*Kapteyn Astronomical Institute, Postbus 800, 9700 AV Groningen, the Netherlands*
[9]*Centre for Astrophysics Research, University of Hertfordshire, Hatfield, Herts AL1 09AB*
[10]*Institute for Advanced Study, Peyton Hall, Princeton, NJ 08544, USA*

Accepted 2008 July 10. Received 2008 June 27; in original form 2008 April 17

ABSTRACT

We analysed two-dimensional maps of 48 early-type galaxies obtained with the SAURON and OASIS integral-field spectrographs using kinemetry, a generalization of surface photometry to the higher order moments of the line-of-sight velocity distribution (LOSVD). The maps analysed include: reconstructed image, mean velocity, velocity dispersion, h_3 and h_4 Gauss–Hermite moments. Kinemetry is a good method to recognize structures otherwise missed by using surface photometry, such as embedded discs and kinematic subcomponents. In the SAURON sample, we find that 31 per cent of early-type galaxies are single component systems. 91 per cent of the multicomponents systems have two kinematic subcomponents, the rest having three. In addition, 29 per cent of galaxies have kinematically decoupled components, nuclear components with significant kinematic twists. We differentiate between slow and fast rotators using velocity maps only and find that fast-rotating galaxies contain discs with a large range in mass fractions to the main body. Specifically, we find that the velocity maps of fast rotators closely resemble those of inclined discs, except in the transition regions between kinematic subcomponents. This deviation is measured with the kinemetric k_5/k_1 ratio, which is large and noisy in slow rotators and about 2 per cent in fast rotators. In terms of E/S0 classification, this means that 74 per cent of Es and 92 per cent of S0s have components with disc-like kinematics. We suggest that differences in k_5/k_1 values for the fast and slow rotators arise from their different intrinsic structure which is reflected on the velocity maps. For the majority of fast rotators, the kinematic axial ratios are equal to or less than their photometric axial ratios, contrary to what is predicted with isotropic Jeans models viewed at different inclinations. The position angles of fast rotators are constant, while they vary abruptly in slow rotators. Velocity dispersion maps of face-on galaxies have shapes similar to the distribution of light. Velocity dispersion maps of the edge-on fast rotators and all slow rotators show differences which can only be partially explained with isotropic models and, in the case of fast rotators, often require additional cold components. We constructed local (bin-by-bin) h_3–V/σ and h_4–V/σ diagrams from SAURON observations. We confirm the classical anticorrelation of h_3 and V/σ, but we also find that h_3 is almost zero in some objects

⋆E-mail: dxk@astro.ox.ac.uk
†Hubble Fellow.

or even weakly correlated with V/σ. The distribution of h_4 for fast and slow rotators is mildly positive on average. In general, fast rotators contain flattened components characterized by a disc-like rotation. The difference between slow and fast rotators is traceable throughout all moments of the LOSVD, with evidence for different intrinsic shapes and orbital contents and, hence, likely different evolutionary paths.

Key words: galaxies: elliptical and lenticular, cD – galaxies: evolution – galaxies: kinematics and dynamics – galaxies: structure.

1 INTRODUCTION

The classification of galaxies both acknowledges the complexity of these celestial objects and attempts to understand their formation and evolution. The Hubble classification of galaxies (Hubble 1936; Sandage 1961; Sandage, Sandage & Kristian 1975; Sandage & Bedke 1994) recognizes the dichotomy between, broadly speaking, disc and ellliptical galaxies, for historical reasons now often called late- and early-types. The classification works well on the late-type galaxies in particular, dividing the class into a number of subgroups which correlate with properties such as bulge-to-disc ratio, morphology of spiral arms, gas and dust content, to name a few, but it fails to bring a physical insight to our understanding of early-types (Tremaine 1987), where the classification is based on apparent shape and thus dependant on viewing angles.

In an effort to eliminate the unsatisfactory situation, Kormendy & Bender (1996) proposed a revision of the Hubble classification. It was based on two discoveries in the 1970s and 1980s, both enabled by an improvement in the technical capabilities of astronomical instruments. A series of papers (Bertola & Capaccioli 1975; Illingworth 1977) showed that bright elliptical galaxies do not rotate as fast as they should, if they were oblate isotropic systems supported by rotation (Binney 1978), whereas less bright and generally smaller systems, including also bulges of spirals, generally agree with such predictions (Kormendy 1982; Kormendy & Illingworth 1982; Davies et al. 1983). A complementary discovery (Bender 1988b; Bender, Doebereiner & Moellenhoff 1988; Bender et al. 1989) that the fast-rotating galaxies are more likely to have discy isophotes, while the slow-rotating galaxies have boxy isophotes, linked again the kinematics and shape of galaxies. Kormendy & Bender (1996) changed the uniformity of early-type galaxies to a dichotomy (discy versus boxy, fast versus slow, brighter versus less bright) and linked the whole Hubble sequence from right- to left-hand side, from Sc–Sb–Sa to S0–E types, where 'rotation decreases in dynamical importance compared to random motions'.

This important step forward introduced a readily measurable parameter related to some physical properties. However, the higher order variations in the isophotal shape (disciness/boxiness) are not measurable at all inclinations regardless of the prominence of the discs (Rix & White 1990), and finally, they are used to infer the dynamical state of the galaxy. This might be a decent approximation, especially if one assumes that all fast-rotating galaxies comprise spheroidal slow-rotating components and discs seen at different inclination (Rix, Carollo & Freeman 1999), but the edge-on observations of spheroidal components in spiral galaxies showed that bulges are rotating fast as well (Kormendy & Illingworth 1982). To complicate things further the updated classification continues to distinguish S0s from Es, keeping a viewing angle dependent definition of S0s (van den Bergh 1990).

The choice of using the fourth-order Fourier term in the isophotometric analysis for classification is natural, because (i) it is much easier to take images of galaxies than to measure their kinematics and (ii) until recently it was not realistic to spectroscopically map their two-dimensional structure. The advent of panoramic integral-field units, such as SAURON (Bacon et al. 2001), is changing the technical possibilities and the field itself; it is now possible to systematically map kinematics of nearby galaxies up to their effective radii. We have observed 72 nearby E, S0 and Sa galaxies as part of the SAURON survey (de Zeeuw et al. 2002, hereafter Paper II). Focusing here on a subsample of 48 early-type galaxies (E,S0), these observations clearly show the previously hinted rich variety of kinematic substructures such as: kinematically decoupled cores, kinematic twists, counterrotating structures and central discs (Emsellem et al. 2004, hereafter Paper III).

Analysing the global properties of the SAURON velocity and velocity dispersion maps, Emsellem et al. (2007, hereafter Paper IX) were able to separate the early-type galaxies into two physically distinct classes of *slow* and *fast* rotators, according to their specific (projected) angular momentum measured within one effective radius, λ_R. This finding augments the view that led to the revision of the classification, but the SAURON observations provide the crucial quantitative data. Moreover, the results of Paper IX suggest a way to dramatically improve on the Hubble classification and substitute S0s and (misclassified) discy ellipticals with one class of fast rotators.

Cappellari et al. (2007, hereafter Paper X) addressed again the issue of orbital anisotropy of early-type galaxies. They constructed the $(V/\sigma, \epsilon)$ diagram (Binney 1978) using an updated formalism (Binney 2005), and compared it with the results from general axisymmetric dynamical models for a subsample of these galaxies (Cappellari et al. 2006, hereafter Paper IV). They found that slow and fast rotators are clearly separated on the $(V/\sigma, \epsilon)$ diagram (unlike Es and S0s), such that slow rotators are round, moderately isotropic and are likely to be somewhat triaxial, while fast rotators appear flattened, span a larger range of anisotropies, but are mostly oblate axisymmetric objects. This finding is in a partial agreement with previous studies which either found round early-type galaxies radially anisotropic (van der Marel 1991), moderately radially anisotropic (Gerhard et al. 2001) or only weakly anisotropic with a range of anisotropies for flattened systems (Gebhardt et al. 2003). The results of Paper X, however, clearly show that intrinsically flatter galaxies tend to be more anisotropic in the meridional plane. The models also indicate that the fast rotators are often two-component systems, having also a flat and rotating, kinematically distinct, disc-like component.

Dynamical models are often time consuming and difficult to construct. Ultimately, one would like to be able to classify galaxies by their observable properties only. Is it possible to learn about the intrinsic shapes of the early-type galaxies from observations only? Surface photometry, being but the zeroth moment of the ultimate observable quantity for distant galaxies, the line-of-sight velocity distribution (LOSVD), cannot give the final answer. It is necessary to look at the other moments of the LOSVD: mean velocity, velocity dispersion and higher order moments, commonly parametrized by Gauss–Hermite coefficients, h_3 and h_4 (Gerhard 1993; van der Marel & Franx 1993), which measure asymmetric and symmetric deviation of the LOSVD from a Gaussian, respectively.

Indeed, in the last dozen years several studies investigated higher moments of the LOSVD of early-type galaxies observing them along one or multiple slits (e.g. Bender, Saglia & Gerhard 1994; van der Marel 1994; van der Marel et al. 1994; Koprolin & Zeilinger 2000; Kronawitter et al. 2000; Halliday et al. 2001; Wegner et al. 2002; Hau & Forbes 2006; Corsini et al. 2008). These studies deepened the dichotomy among early-type galaxies showing that fast-rotating galaxies with discy isophotes also exhibit an anticorrelation between h_3 and V/σ. This is consistent with these galaxies being made of two components: a bulge and a disc. The symmetric deviations, on the other hand are usually smaller than asymmetric ones, and somewhat positive in general. In addition, the observed higher order moments of the LOSVD can be used to constrain the possible merger scenarios of early-type galaxies and their formation in general (e.g. Balcells 1991; Bendo & Barnes 2000; González-García, Balcells & Olshevsky 2006; Naab, Jesseit & Burkert 2006; Jesseit et al. 2007). However, observations along one or two slits are often not able to describe the kinematical richness of early-type galaxies.

In this paper we use *kinemetry* (Krajnović et al. 2006), a generalization of surface photometry to all moments of the LOSVD, to study SAURON maps of 48 early-type galaxies. The purpose of this paper is to investigate observational clues from resolved two-dimensional kinematics for the origin of the differences between the slow and fast rotators.

In Section 2 we briefly remind the reader of the SAURON observations and data reduction. Section 3 describes the methods and definitions used in this paper. The main results are presented in Section 4. In Section 5 we offer an interpretation of the results and we summarize the conclusions in Section 6. In Appendix A we discuss the influence of seeing on the two-dimensional kinematics and in Appendix B we present the radial profiles of the kinemetric coefficients used in this study.

2 SAMPLE AND DATA

In this paper we used the data from the SAURON sample which was designed to be *representative* of the galaxy populations in the plane of ellipticity, ϵ, versus absolute B-band magnitude M_B. The sample and its selection details are presented in Paper II. In this study we focus on the 48 galaxies of the SAURON E + S0 sample.

SAURON is an integral-field spectrograph with a field of view (FOV) of about 33×41- and 0.94×0.94-arcsec^2 square lenses, mounted at the William Herschel Telescope. Complementing the SAURON large-scale FOV, we probed the nuclear regions of a number of galaxies with OASIS, then mounted at Canada–Hawaii–France Telescope, a high spatial resolution integral-field spectrograph, similarly to SAURON based on the TIGER concept (Bacon et al. 1995). The FOV of OASIS is only 10×8 arcsec^2, but the spatial scale is 0.27×0.27 arcsec^2, fully sampling the seeing-limited point spread function (PSF) and providing on average a factor of 2 improvement in spatial resolution over SAURON. The spectral resolution of OASIS is, however, about 20 per cent lower than that of SAURON, and only a subsample of the SAURON galaxies was observed.

In this paper we are investigating the stellar kinematics of early-type galaxies. Paper III and McDermid et al. (2006, hereafter Paper VIII) discuss the extraction of kinematics and construction of maps of the mean velocity V, the velocity dispersion σ, and the Gauss–Hermite moments h_3 and h_4 in great detail. All maps used in this paper are Voronoi binned (Cappellari & Copin 2003) to the same signal-to-noise ratio. The SAURON kinematic data used here are of the same kinematic extraction as in Paper X with the latest improvement on the template mismatch effects in higher moments of the LOSVD. The SAURON mean velocity maps are repeated in this paper for the sake of clarity, but we encourage the reader to have copies of both Paper III and Paper VIII available for reference on other moments of the LOSVD.

3 METHOD AND DEFINITIONS

Maps of the moments of the LOSVD offer a wealth of information, but also suffer from complexity. It is difficult, if not impossible, to show error bars for each bin on the map, and the richness of the maps can lead to the useful information being lost in detail. As in the case of imaging, it is necessary to extract the useful information from the maps to profit from their two-dimensional coverage of the objects. In this section we describe the method used to analyse the maps and discuss definitions utilized throughout the paper.

3.1 Kinemetry

Krajnović et al. (2006) presented kinemetry, as a quantitative approach to analysis of maps of kinematic moments. Kinemetry is a generalization of surface photometry to the higher order moments of the LOSVD. The moments of the LOSVD have odd or even parity. The surface brightness (zeroth moment) is even, the mean velocity (first moment) is odd, the velocity dispersion (second moment) is even, etc. Kinemetry is based on the assumption that for the odd moments the profile along the ellipse satisfies a simple cosine law, while for the even moments the profile is constant (the same assumption is also used in surface photometry). Kinemetry derives such best-fitting ellipses and analyses the profiles of the moments extracted along these by means of harmonic decomposition. It follows from this that the application of kinemetry on even moments is equivalent to surface photometry resulting in the same coefficients for parametrization of the structures (e.g. position angle, ellipticity and fourth-order harmonics).

Application of kinemetry on odd maps such as velocity maps[1] provides radial profiles of the kinematic position angle $\mathrm{PA_{kin}}$, axis ratio or flattening, $q_{\mathrm{kin}} = b/a$ (where b and a are lengths of minor and major axis, respectively), and odd harmonic terms obtained from the Fourier expansion (since velocity is an odd map, even terms are,

[1]It is customary in the literature to refer to the maps of mean velocity as *velocity fields*. Sometimes, due to the specific shape of contours of constant velocities, velocity maps are referred to as *spider diagrams* (e.g. van der Kruit & Allen 1978). Two-dimensional representations of the next moment are, however, usually referred to as velocity dispersion maps. Instead of alternating between *fields* and *maps* we choose to call all two-dimensional representations of the LOSVD maps: velocity map, velocity dispersion map, h_3 map, etc.

in principle, not present, while in practice are very small and usually negligible). In the case of stellar velocity maps, the dominant kinemetry term is $k_1 = \sqrt{a_1^2 + b_1^2}$, representing the velocity amplitude, where a_1 and b_1 are the first sine and cosine terms, respectively. The deviations from the assumed simple cosine law are given by the first higher order term that is not fitted, $k_5 = \sqrt{a_5^2 + b_5^2}$, usually normalized with respect to k_1. These four parameters form the basis of our analysis because they quantify the kinematical properties of the observed galaxies: orientation of the map (a projection of the angular momentum), opening angle of the isovelocity contours, the amplitude of the rotation and the deviation from the assumed azimuthal variation of the velocity map. For the other moments of the LOSVD one could derive similar quantities, depending on the parity of the moment. As will be discussed below, we focus on kinemetry coefficients that describe velocity maps in detail and some specific kinemetry coefficients from the maps of the higher order moments. A detailed description of the method, error analysis and parameters is given in Krajnović et al. (2006).

3.2 Radial profiles

Kinemetric radial profiles can be obtained along ellipses of different axial ratios and position angles. At each radius there is the best-fitting ellipse, along which a profile of the kinematic moment will have a certain shape: it follows a cosine or it is constant, for odd and even moments, respectively. If this is the case, the higher order Fourier terms are non-existent or at least negligible for such an ellipse.

In the case of even moments, the best-fitting ellipses describe the underlying isocontours, like isophotes in the case of surface photometry, or contours of constant velocity dispersion, iso-σ contours. In the case of odd moments, this is somewhat more difficult to visualize, but the axial ratio of the best-fitting ellipse is related to the opening angle of the isovelocity contours: the larger the axial ratio, the more open is the spider diagram of the velocity map.

In this study, kinemetry is used for extraction of parameters in the following ways.

(i) We apply kinemetry to SAURON reconstructed images of galaxies, which are obtained by summing the spectra along the spectral direction at each sky position. This is equivalent to low-resolution surface photometry on galaxies from the sample. We focus on the photometric position angle $\mathrm{PA_{phot}}$ and photometric axial ratio, related to ellipticity as $q_{\mathrm{phot}} = 1 - \epsilon$. In this case, kinemetry is used in its *even* mode, where even harmonics are fitted to the profiles extracted along the best-fitting ellipses.

(ii) We use kinemetry to derive radial profiles of the four parameters that describe velocity maps: $\mathrm{PA_{kin}}$, q_{kin}, k_1 and k_5. In this case, kinemetry is applied to the maps in its *odd* mode, when only odd Fourier harmonics are fit to the profiles extracted along the best-fitting ellipses, which are, in general, different from the best-fitting ellipse of (i). In some cases when it is not possible to determine the best-fitting ellipse we run kinemetry on circles (see below).

(iii) Kinemetry is applied to velocity dispersion maps, using the *even* mode as in (i). In this case, however, the parameters of the ellipses used to extract profiles were fixed to the best-fitting values of surface photometry obtained in (i). (iv) Maps of Gauss–Hermite coefficients h_3 and h_4 were also parametrized using kinemetry in *odd* and *even* mode, respectively. In both cases, we used the best-fitting ellipses from the lowest *odd* (velocity map) and *even* moment (reconstructed image), respectively.

Before proceeding it is worth explaining in more detail our decision not to use kinemetry to fit the ellipses in some cases. Under (ii) we mentioned that on some velocity maps it was necessary to run kinemetry on circles. In general, the mean stellar velocity has an odd parity, and its map, in an inclusive triaxial case, will be point-antisymmetric. Certain maps, however, do not follow this rule, having no detectable net rotation, e.g. NGC 4486, or the inner part of NGC 4550. In the latter case, the zero velocity in the inner part can be explained by the superposition of two counterrotating stellar components as advocated by Rubin, Graham & Kenney (1992) and Rix et al. (1992), where the mass of the counterrotating component is about 50 per cent of the total mass (Paper X). In other cases the non-rotation could be a result of dominant box orbits which have zero angular momentum. The basic assumption of kinemetry for odd kinematic moments therefore breaks down resulting in velocity maps that appear noisy and one cannot expect reasonable results.

In practice, this means that the best-fitting ellipse parameters for maps without net rotation will not be robustly determined (degeneracy in both $\mathrm{PA_{kin}}$ and q_{kin}) while the higher harmonic terms will be large and meaningless. Specifically, k_5 will have high values. We partially alleviate this degeneracy by first running an unconstrained kinemetry fit on stellar velocity maps and identifying maps where $k_5/k_1 > 0.1$ and corresponding radii where it occurs. At these radii we rerun kinemetry, but using circles for extraction of velocity profiles and Fourier analysis. In this way we set the axial ratio $q_{\mathrm{kin}} = 1$ in order to break the degeneracy. Although the k_5/k_1 term cannot be directly compared with the k_5/k_1 term obtained from a best-fitting ellipse, in this case, if there is any indication of odd parity in the map, we can still determine the local amplitude of rotation k_1, and give a good estimate for $\mathrm{PA_{kin}}$.

The other note refers to items (iii) and (iv). Although, in principle, it would be possible to run kinemetry freely on the velocity dispersion maps, or maps of higher Gauss–Hermite moments (e.g. h_3 and h_4), the noise in the data is too high to give trustworthy results for the whole sample. By setting the shape of the curve to the best-fitting ellipses of the corresponding lowest odd or even moment, the harmonic terms of kinemetry quantify the differences between these even and odd moments of the LOSVD.

An example of expected differences can be visualized comparing the isophotes of the surface brightness and the stellar velocity dispersion maps of NGC 2549 and 4473 (Fig. 1). On both images isophotes are aligned with the vertical (y) axis of the maps. In the case of NGC 2549 the contours of constant velocity dispersion seem to be perpendicular to the isophotes, at least within the central 10 arcsec, while in the rather unusual case of NGC 4473, the high values of velocity dispersion have the same orientation as the isophotes. The physical explanation of these striking differences should be looked for in the internal orbital structure. We postpone this discussion to Section 4.4.

The noise and irregular shape of iso-σ contours decrease the usefulness of fitting for the velocity dispersion contours. Extracting harmonic terms along the isophotes, however, can yield a clear signal of the different shape of these two moments. An extracted velocity dispersion profile in these two cases (e.g. along the second brightest isophote shown in Fig. 1) will go through two maxima and two minima. The minima and maxima of these two profiles will be out of phase, because along the major axis in NGC 2549 there is a decrease in velocity dispersion while in NGC 4473 there is an increase. The decomposition of these two profiles will give different amplitudes to the harmonic terms. Specifically, b_2 (cosine) term will be the most influenced, because this term is related to the error in the axial ratio (Jedrzejewski 1987), and the shapes such

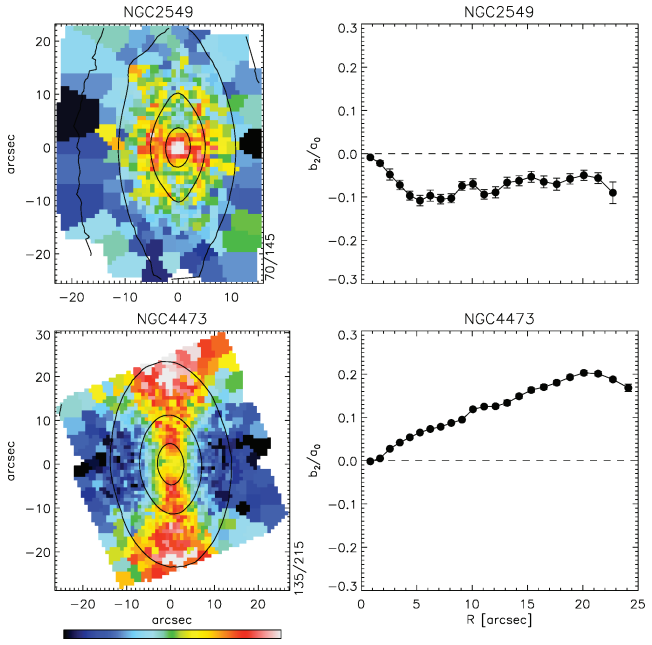

Figure 1. Left-hand panel: Voronoi binned stellar velocity dispersion maps of NGC 2549 (top) and NGC 4473 (bottom). Overplotted lines are isophotes. In the lower right-hand corner of each map are values that correspond to minimum and maximum colours on the colour bar. Right-hand panel: Radial profiles of b_2/a_2 kinemetry terms for NGC 2549 (top) and NGC 4473 (bottom).

as in NGC 2549 and 4473 will give negative (iso-σ rounder than isophotes) and positive (iso-σ flatter than isophotes) b_2, respectively. An alternative way to visualize the difference between these two maps based on the values of b_2 is to consider that a negative b_2, corresponds to a decrease of the σ at the major axis of the best-fitting ellipse compared to the σ measured at the minor axis of the best-fitting ellipse (NGC 2549). In contrast, a positive b_2 corresponds to an increased value of the σ at the major axis position of the best-fitting ellipse (NGC 4473). By monitoring these harmonic terms it is possible to quantify the shape difference between the observed zeroth and second moments of the LOSVD.

3.3 Definition of structures on stellar velocity maps

A few kinemetric profiles are able to describe a wealth of information from the maps. Specifically, we wish to use them to highlight the kinematic structures on the maps and to recognize hidden kinematic components. Here we present a set of quantitative criteria for describing features on the stellar velocity maps. Some of the criteria are dependent on the quality of the data and they should be modified if used on maps obtained with other IFUs. The following rules were presented by Krajnović et al. (2006) and Paper IX, but here we list them for the sake of clarity.

A single velocity map can contain a number of kinematic components. Often they are easily recognisable by visual inspection. In a quantitative way we differentiate between the following maps.

(i) *Single component* (SC) map: having a radially constant or slow varying $\mathrm{PA_{kin}}$ and q_{kin} profiles.

(ii) *Multiple component* (MC) map: characterized with an abrupt change in either $\Delta q_{\mathrm{kin}} > 0.1$, or $\Delta \mathrm{PA_{kin}} > 10^\circ$, or a double hump in k_1 with a local minimum in between, or a peak in k_5 where $k_5/k_1 > 0.02$.

MC maps are clearly more complex than SC maps. The above values for changes to the kinemetric coefficients are used to determine the extent of each subcomponent (components C_1, C_2 and C_3 with radii R_{12} and R_{23} between them). Each subcomponent can be described as being of the following type (limiting values apply for the SAURON dataset).

(i) *Disc-like rotation* (DR): defined when the higher order harmonic $k_5/k_1 < 0.02$, while the variation of q_{kin} and $\mathrm{PA_{kin}}$ is less than 0.1 and 10°, respectively. Note that this name *does not* imply that the object is a disc intrinsically.

(ii) *Low-level velocity* (LV): defined when the maximum of k_1 is lower than $15\,\mathrm{km\,s^{-1}}$. A special case is *central low-level velocity* (CLV) when LV occurs in the central kinematical component on the map.

(iii) *Kinematic misalignment* (KM): defined when the absolute difference between the photometric $\mathrm{PA_{phot}}$ and kinemetric position $\mathrm{PA_{kin}}$ angles is larger than 10°.

(iv) *Kinematic twist* (KT): defined by a smooth variation of the kinematics position angle $\mathrm{PA_{kin}}$ with an amplitude of at least 10° within the extent of the kinematic component.

(v) *Kinematically decoupled component* (KDC): if there is an abrupt change in $\mathrm{PA_{kin}}$, with a difference larger than 20° between two adjacent components, or if there is an outer LV component (in which case the measurement of $\mathrm{PA_{kin}}$ is uncertain). A special case of KDCs are *counterrotating cores* (CRC) where $\Delta \mathrm{PA_{kin}}$ between the components is 180° (within the uncertainties).

Most of the above definitions are new, arising from two-dimensional maps which offer a more robust detection of structures. The definition of KDC is, however, similar to the one used in the past (e.g. Bender 1988a; Statler 1991), where the two-dimensional coverage enables a determination of the orientation of the kinematic components. It should be noted that classification of a kinematic component as a CLV is strongly dependent on the spatial resolution of the instrument. As will be seen later, higher spatial resolution can change the appearance and therefore the classification of the components.

Similarly, it should be stressed that the limiting values used for these definitions are geared towards the SAURON data. The OASIS data, due to different instrumental properties and observing set-up, will have somewhat different limiting values, mostly arising in the higher order Fourier terms. For example, the mean uncertainty of k_5/k_1 term for the OASIS sample is 0.033, significantly higher compared to the one for the SAURON sample (0.015). In order to treat consistently the two data sets, we adopt a somewhat more conservative value of 0.04 as the limiting values for k_5/k_1 in definition of DR component when estimated from the OASIS data.

While abrupt changes in the orientation, axial ratio, or velocity amplitude are intuitively clear as evidences for separate kinematic components, the k_5/k_1 as an indicator of components is more complex to comprehend. Still, the simple models of two kinematic components rotating at a given relative orientation give rise to k_5/k_1 term in the kinemetric expansion in the region where these components overlap (Krajnović et al. 2006). Since we measure luminosity-weighted velocities, the position and extent of the raised k_5/k_1 region depends on relative luminosity contributions of the components, marking the transition radii between the components and not their start or end. Furthermore, it is also necessary to distinguish between high k_5/k_1 due to a superposition of kinematic components (a genuine signal) and high k_5/k_1 originating from noisy maps, such as maps with no detectable rotation (e.g. NGC 4486) or large bin-to-bin variations (e.g. OASIS map of NGC 3379). For our data, when

the signal in k_5 is 10 per cent of k_1, we consider the noise too high and the k_5/k_1 ratio not usable for detecting individual components.

3.4 Seeing and quantification of kinematic components

Robust estimates of the number of subcomponents in velocity maps and their sizes are influenced by three major factors: data quality, physical properties and seeing. While the data quality is described by measurement uncertainties, and in that sense it is quantifiable to some extent, the other two factors are more complex. By 'physical properties' we assume physical processes that hide kinematic information from our view, such as specific orientation of the object, dust obscuration or simply the fact that we are measuring luminosity-weighted quantities and we might miss kinematic components made up of stars that constitute a low luminosity fraction of the total population.

The influence of seeing is particularly relevant for subcomponents in the centres of galaxies. In Appendix A we tested the dependence of the kinemetric coefficients on representative seeings, for velocity maps viewed at different orientations. This exercise showed that: (i) $\mathrm{PA_{kin}}$ and k_5/k_1 are not significantly influenced by the seeing, (ii) the amplitude and, to a minor extent, the shape of k_1 are somewhat influenced by the seeing and (iii) the axial ratio q_{kin} can be strongly influenced by the seeing (Fig. A2). In addition to these conclusions, the test showed that the inclination of an object is also a factor contributing to the change of the intrinsic q_{kin}, and to a minor extent, k_1 profiles, where higher inclinations are particularly influenced by the seeing effects.

In practice, this means that the change in q_{kin} is a less robust indicator of kinematic components. We found that more robust indicators are abrupt changes in k_5/k_1 and $\mathrm{PA_{kin}}$ profiles, double humps in k_1 profiles or decrease of k_1 amplitude below our detection limit for rotation. We used these as estimates of the sizes of kinematic components. It should be, however, noted that the size of a component is just a luminosity-weighted estimate, originating from a superposition of luminosities of individual components, and the component can intrinsically extend beyond that radius. Only detailed dynamical models could give a more robust estimate of the internal orbital structure.

3.5 Determination of global and average values

In addition to radial profiles we present in this paper a number of average quantities. Similar luminosity-weighted quantities have already been derived in Papers IX and X: global $\mathrm{PA_{kin}}$, global $\mathrm{PA_{phot}}$, average ϵ. In this study we use the velocity maps to determine the luminosity-weighted average $\langle \mathrm{PA_{kin}} \rangle$, $\langle q_{\mathrm{kin}} \rangle$ and $\langle k_5/k_1 \rangle$ for the whole map and for each kinematic component. We also measured the luminosity-weighted $\langle \mathrm{PA_{phot}} \rangle$, $\langle q_{\mathrm{phot}} \rangle$ from the reconstructed images (both global and for each component), $\langle b_2/a_0 \rangle$ from velocity dispersion maps and average values of h_4 (measured as the a_0 harmonic term) from h_4 maps. In practice, we do this following the expression from Paper IX. The mean $\langle G \rangle$ of a quantity $G(R)$ derived from its sampled radial profiles can be approximated with

$$\langle G \rangle \sim \frac{\sum_{k=1}^{N} q(R_k) F(R_k) G(R_k) \left(R_{\mathrm{out},k}^2 - R_{\mathrm{in},k}^2\right)}{\sum_{k=1}^{N} q(R_k) F(R_k) \left(R_{\mathrm{out},k}^2 - R_{\mathrm{in},k}^2\right)}, \quad (1)$$

where $q(R_k)$ and $F(R_k)$ are the axial ratio and the surface brightness of the best-fitting ellipse, with semimajor axis R_k. Equation (1) is based on an expression defined in Ryden et al. (1999). The uncertainties of these average values are calculated in the standard way as the sum of the quadratic differences between the average value and the value at each position R_k.

In Paper X the global $\mathrm{PA_{kin}}$ was derived using the formalism from appendix C in Krajnović et al. (2006). This approach differs from the one described here in the sense that it is less sensitive to the kinematic structures in the central region, such as abrupt changes of PA in case of a KDC. That approach is well suited for making global comparisons between $\mathrm{PA_{kin}}$ or $\mathrm{PA_{phot}}$, such as global kinematic misalignment, when it is required that they are measured on large scales to avoid influence of local perturbations in the nuclear regions (e.g. seeing, dust, bars). In this study, however, we want to compare the radial properties of different moments of the LOSVD and for that reason we use the approach of Paper IX to all measured quantities. Note that for the purpose of the direct comparison we measured both kinematic and photometric quantities on the SAURON data, in contrast with Papers IX and X.

4 RESULTS

In this section we present the results of kinemetric analysis of the LOSVD moments maps. We look at the presence of kinematic substructures in velocity maps (Section 4.1), properties of radial profiles of $\mathrm{PA_{kin}}$, k_1, σ (Section 4.2), comparison between q_{kin} and q_{phot} (Section 4.3), the shape difference between isophotes and iso-σ contours (Section 4.4) and properties of h_3 and h_4 Gauss–Hermite moments (Section 4.5) with the purpose to investigate the internal structure of SAURON galaxies. Kinemetry probes local characteristics of galaxies, and we wish to link those with the global properties described in Papers IX and X. In this analysis, the most useful is the first moment of the LOSVD, the mean velocity, because it is a moment rich in structure and with the strongest signal. We present the kinemetric profiles of this moment in Appendix B. Although kinemetry is performed on other moments of the LOSVD, we discuss the dominant terms only.

4.1 Substructures on the velocity maps

Looking at the kinemetric profiles of 48 SAURON galaxies (Fig. B1) the following general conclusions can be made.

(i) $\mathrm{PA_{kin}}$ profiles are in general smooth and often constant (e.g. NGC 2974) or mildly varying (e.g. NGC 474). In some cases there are abrupt changes of up to 180° within 1–2 arcsec (e.g. NGC 3608).

(ii) Profiles of the axial ratio q_{kin} are generally smooth and often similar to q_{phot} profiles (e.g. NGC 1023, 3384, 4570).

(iii) There is a variety of k_1 profiles, most of them rise and flatten, but some continue to rise, while some drop (e.g. NGC 4278, 4477 and 4546).

(iv) Considering the k_5/k_1 radial dependence, there are three kinds of objects: those that have the ratio below 0.02 along most of the radius (e.g. NGC 2974), those that have the ratio greater than 0.1 along most of the radius (e.g. NGC 4374) and those that have the ratio below 0.02 with one (or more) humps above this value (e.g. NGC 2549).

(v) Objects with $k_5/k_1 > 0.1$ along a significant part of the profile from SAURON data are all classified as slow rotators in Paper IX (e.g. NGC 4486).

A further step in understanding the complex velocity maps can be made by applying definitions of kinemetric groups (see Section 3.3) to the radial profiles. They are summarized in Table 1. There are

Table 1. Kinemetric properties of the 48 E and S0 SAURON galaxies.

Galaxy (1)	Group (2)	N_C (3)	R_{12} (4)	R_{23} (5)	C_1 (6)	C_2 (7)	C_3 (8)	KM (9)	Rotator (10)	Comment (11)
NGC 0474	MC	2	7	–	DR	DR	–	KM(1,2)	F	KT between C_1 and C_2
NGC 0524	SC	1	–	–	DR	–	–	–	F	Possible C_2 beyond $r = 12$ arcsec
NGC 0821	SC	1	–	–	DR	–	–	–	F	Flat k_1 profile
NGC 1023	SC	1	–	–	KT	–	–	–	F	$k_5/k_1 < 0.02$,
NGC 2549	MC	2	13	–	DR	DR	–	–	F	C_2: flat k_1 profile
NGC 2685	SC	1	–	–	DR	–	–	–	F	–
NGC 2695	MC	2	7	–	DR	DR	–	–	F	–
NGC 2699	MC	2	6	–	DR	DR	–	KM(1,–)	F	C_2: flat k_1 profile
NGC 2768	SC	1	–	–	–	–	–	–	F	$r \lesssim 10$ arcsec rigid body rotation; $k_5/k_1 < 0.02$ for $r > 10$ arcsec
NGC 2974	SC	1	–	–	DR	–	–	–	F	–
NGC 3032	MC (CLV)	2	2.5	–	LV	DR	–	–	F	CRC in OASIS map
NGC 3156	SC	1	–	–	DR	–	–	–	F	–
NGC 3377	SC	1	–	–	KT	–	–	–	F	$k_5/k_1 < 0.02$ over the map
NGC 3379	SC	1	–	–	DR	–	–	–	F	–
NGC 3384	MC	2	10	–	DR	DR	–	KM(–,2)	F	–
NGC 3414	MC (KDC)	2	10	–	DR	LV	–	KM(–,2∗)	S	CRC
NGC 3489	MC	2	6	–	DR	DR	–	–	F	–
NGC 3608	MC (KDC)	2	10	–	DR	LV	–	KM(–,2∗)	S	CRC
NGC 4150	MC (CLV)	3	3.5	9.5	LV	–	DR	KM(1,–,–)	F	KDC in OASIS map with $r_{\rm size} = 1.5$ arcsec
NGC 4262	MC	2	9	–	DR	–	–	KM(1,2)	F	–
NGC 4270	MC	2	6	–	–	–	–	–	F	Possible there components
NGC 4278	MC	2	16	–	DR	–	–	KM(–,2)	F	C_2: decreasing k_1 profile
NGC 4374	SC	1	–	–	LV	–	–	KM∗	S	–
NGC 4382	MC (CLV)	3	2	14.5	LV	DR	DR	KM(1,–,–)	F	CRC in OASIS map, KT between C_1 and C_2
NGC 4387	MC	2	7	–	DR	DR	–	–	F	Decreasing k_1 beyond $r = 13$ arcsec
NGC 4458	MC (KDC)	2	3	–	–	LV	–	KM(–,2∗)	S	–
NGC 4459	MC	2	12	–	DR	DR	–	KM(1,–)	F	–
NGC 4473	MC	2	10	–	DR	–	–	–	F	C_1: possible KT. C_2: decreasing k_1 profile.
NGC 4477	SC	1	–	–	DR	–	–	KM	F	–
NGC 4486	SC	1	–	–	LV	–	–	KM∗	S	–
NGC 4526	MC	2	11	–	DR	–	–	–	F	C_2: decreasing k_1 profile
NGC 4546	MC	2	9	–	DR	DR	–	KM(1,–)	F	C_2: flat k_1 profile
NGC 4550	SC	1	–	–	LV	–	–	KM∗	S	Two cospatial counterrotating discs not detected
NGC 4552	MC (KDC)	2	4	–	KT	–	–	KM(1,2)	S	Flat $k_1 = 15\,{\rm km\,s^{-1}}$ over the map
NGC 4564	SC	1	–	–	DR	–	–	–	F	–
NGC 4570	MC	2	8	–	DR	DR	–	–	F	–
NGC 4621	MC (KDC)	2	4	–	DR	DR	–	KM(1,–)	F	CRC in OASIS with r∼1.5 arcsec
NGC 4660	MC	2	7	–	DR	DR	–	–	F	–
NGC 5198	MC (KDC)	2	2.5	–	–	KT	–	KM(1∗,2∗)	S	C_2: LV between 2.5 and 10 arcsec
NGC 5308	MC	2	7	–	DR	DR	–	–	F	No signature of C_2 in k_5/k_1
NGC 5813	MC (KDC)	2	12	–	DR	LV	–	KM(–,2∗)	S	–
NGC 5831	MC (KDC)	2	8	–	DR	LV	–	KM(–,2∗)	S	–
NGC 5838	MC	2	6	–	DR	DR	–	–	F	No signature of C_2 in k_5/k_1
NGC 5845	MC	2	4.5	–	DR	DR	–	–	F	–
NGC 5846	SC	1	–	–	LV	–	–	KM∗	S	–
NGC 5982	MC (KDC)	2	3.5	–	–	LV	–	KM(1,–)	S	C_2: LV is between 2 and 8 arcsec
NGC 7332	MC (KDC)	3	3	12	KT	DR	DR	KM(1,–,–)	F	C_2: continuously increasing k_1; KDC only in PA change
NGC 7457	MC (CLV)	2	3	–	KT	DR	–	KM(1,2)	F	C_2: continuously increasing k_1

Notes: (1) Galaxy identifier; (2) kinematic galaxy group: see text for details; (3) number of kinematic components; (4) transition radius between the first and second components (arcsec); (5) transition radius between the second and third components (arcsec); (6, 7 and 8) kinematic group for the first second and third components; (9) local kinematic misalignment between luminosity-weighted averages of PA_{kin} and PA_{phot}: numbers refer to the kinematic component and * notes that the PA_{kin} was determined in the region with k_1 mostly below $15\,{\rm km\,s^{-1}}$; (10) rotator class: S – slow rotator, F – fast rotator; (11) comment.

15 galaxies characterized as SC (31 per cent),[2] the rest being MC galaxies (69 per cent) of which 10 have KDC (21 per cent) and four have CLV (8 per cent). Higher resolution observations with OASIS, however, show that all SAURON CLVs are in fact small KDCs and, moreover, CRCs (Paper VIII). This means that there are actually 14 (29 per cent) KDCs in the SAURON sample. Kinematic profiles of the OASIS data also clearly show structures that are partially resolved in the SAURON observations, such as KDC (NGC 4621, 5198, 5982) or corotating components which often have larger amplitudes of rotation in the OASIS data, corresponding to the nuclear discs visible on the *Hubble Space Telescope* (*HST*) images. The

[2]Although NGC 4550 is made of two counterrotating and cospatial discs (Section 3.2), it is formally characterized as a SC galaxy due to its low velocity within the SAURON FOV.

effects of specific nuclear kinematics, related mean ages of the components and possible different formation paths were previously discussed in Paper VIII.

In addition to this grouping of the velocity maps, we can also describe the kinematic components. Out of 15 SC galaxies, eight are DR (53 per cent), two are KT (13 per cent) and four are LV (27 per cent), while the remaining galaxy (NGC 2768) is a rather special case of a solid body rotator (see below). The majority of MC galaxies have only two kinematic components (30 or 91 per cent), but there are some with three kinematic components (3 or 9 per cent). Many of the components are similar in properties. If the inner component (C_1) is DR then the second component (C_2) is also a DR. If C_1 has a more complex kinematic structures (KDC, LV, KT), C_2 or C_3 will in most cases still be a DR. Exceptions are found in a few cases when C_2 is not rotating and can be described as LV. In some cases components may show KT, but their k_5/k_1 ratio is less than or equal to 0.02. Counting all galaxies that have at least one component with $k_5/k_1 \lesssim 0.02$, the number of systems with DR-like characteristics rises to 35 (73 per cent). In terms of E/S0 classification, this means that 74 per cent of Es and 92 per cent of S0s have components with disc-like kinematics

Using the resolving power of the OASIS data we can go even further: allowing for large error bars and allowing for considerable uncertainty of component boundaries, virtually every galaxy that shows rotation (including parts of KDCs) has at least one region with $k_5/k_1 \lesssim 0.02$ (0.04 in OASIS). This can be seen in Fig. 2 that shows luminosity-weighted average of k_5/k_1 ratio versus the maximum rotational amplitude k_1 for all fast rotators measured on the SAURON data. The large uncertainties in some cases reflect the multiple component nature of fast rotators, because k_5/k_1 ratio rises in the transition region between components (Krajnović et al. 2006). Notably, both average values and uncertainties rise as the maximum rotation velocity decreases. This suggests a more complex structure (more components, larger difference between components) in galaxies with lower amplitude of rotation.

We estimated local kinematic misalignment for each kinematic component. The results show that a total of 25 galaxies (52 per cent of the sample) have some evidence of KM. It should, however, be kept in mind that it is difficult to determine the sense of rotation for LV components. Ignoring galaxies with an LV in the single component or in the second component, we are left with 15 galaxies with kinematic misalignments. Of these, 13 galaxies show misalignment in the first component, and seven in the second component. Moreover, only five galaxies show misalignment in two components, as a global property within the SAURON FOV.

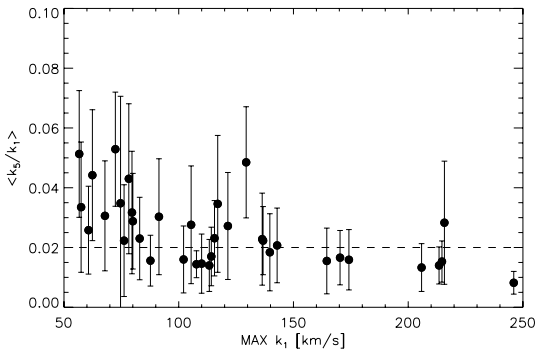

Figure 2. A relation between the maximum amplitude of rotation and luminosity-weighted average of k_5/k_1 ratio, which measures departures from the cosine law for velocity profiles extracted along the best-fitting ellipse. All points belong to fast rotators.

As it can be seen from the kinemetric profiles there are special cases for which kinemetry is not able to determine the characteristic parameters robustly. This, in general, occurs when velocity drops below $\sim$15 km s^{-1} (e.g. NGC 4486, 4550), and it is not surprising since these maps also often lack odd parity, an expected property of the first moment of the LOSVD. As discussed in Krajnović et al. (2006), another exception is the case of solid body rotation for which the isocontours are parallel with the zero-velocity curve. In the SAURON sample this is seen in NGC 2768. Since the velocity isocontours are parallel the axial ratio and the position angle are poorly defined and in practice strongly influenced by noise in the data. Determination of the best-fitting ellipse parameters for the solid body rotation is degenerate. From these reasons this galaxy should also be considered with care when comparing with kinemetry results for other objects.

4.2 Fast versus slow rotators

As stated above, all galaxies with $k_5/k_1 > 0.1$ along a significant part of the profile from SAURON data are classified as slow rotators in Paper IX. To some extent this is expected since slow rotators in general show very little rotation and kinemetry assumptions are not satisfied. The origin of the noise in the maps of slow rotators, which generates large k_5/k_1, is likely reflecting a special internal structure, and, in principal, does not come from technical aspects of the observations. Even velocity maps with low amplitude of rotation could show regular spider diagrams (e.g. discs seen at very low inclinations) observed at the same signal-to-noise ratio. The one-to-one relation between slow rotators and objects with large higher order harmonic terms is significant since the slow/fast rotator classification is based on both velocity and velocity dispersion maps and reflects the internal structure.

The OASIS data cover only a small fraction of the effective radius and do not show this relationship. The slow rotators NGC 3414, 3608, 5813 and 5982 show considerable rotation because the KDC is covering the full OASIS FOV, while the central regions of the fast rotators NGC 2768, 3032 and 3379 still have small amplitudes of rotation and high (and noisy) k_5/k_1 ratios.

The velocity maps of the 12 slow-rotating galaxies in our sample can be described either as LV or as KDC + LV. In that respect, four slow rotators are SC systems (NGC 4374, 4486, 4550 and 5846) which do not show any detectable rotation (at SAURON resolution) and the other eight are MC systems where C_1 is a KDC and C_2 is an LV. In between these two cases is NGC 4552 with a rather constant rotation velocity of 15 km s^{-1}, the boundary level for LV, and the C_1 between a KDC and a large KT. The other three quarters of galaxies in the SAURON sample are fast rotators. Only one-third of them are described as SC, but as shown above (Section 4.1) all fast rotators have components with kinematics that can be described as DR. Moreover, in the case of some slow rotators with small, but not negligible rotation in the centres (KDC), the higher resolution OASIS data were able to ascertain that these components have near to DR properties (within often large uncertainties).

Fig. 3 has three panels highlighting most obvious kinematic properties of slow and fast rotators. The top panel shows radial variations of the kinematic position angles, PA_{kin}, which are present in various forms, ranging from minor twists in the nuclei, through abrupt jumps at the end of KDCs, to almost random changes with radius. However, only PA_{kin} of slow rotators are characterized by strong and rapid changes. Fast rotators show remarkably constant PA_{kin}.

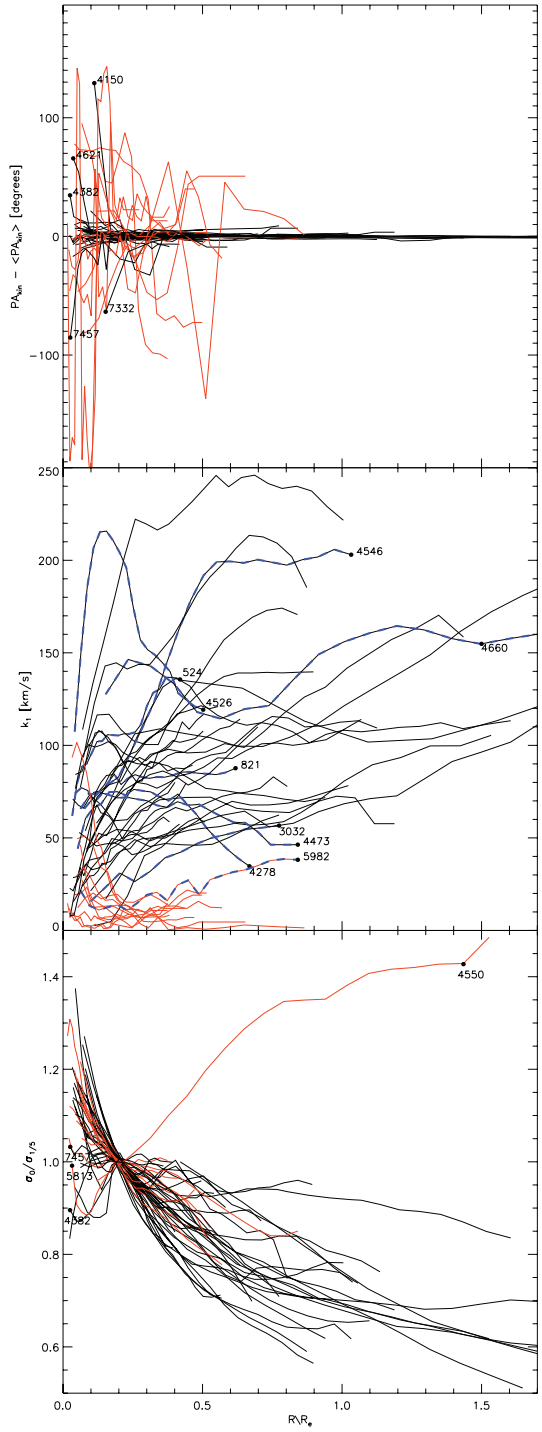

Figure 3. Radial profiles of (from top to bottom) $\mathrm{PA_{kin}} - \langle \mathrm{PA_{kin}} \rangle$, k_1 and σ_0 from the SAURON data. $\langle \mathrm{PA_{kin}} \rangle$ are luminosity-weighted averages of $\mathrm{PA_{kin}}$ profiles. σ_0 profiles are normalized at $R_e/5$. The profiles of slow and fast rotators are coloured in red and black, respectively. In the middle panel dashed blue lines are overplotted to guide the eye for the cases with specific profiles as mentioned in text.

If twists are present in $\mathrm{PA_{kin}}$ of fast rotators, they are small in amplitude ($\lesssim 30^\circ$) and confined to the nuclear region in shapes of physically small KDCs (NGC 4150, 4382, 4621, 7332, 7457). Slow rotators on the other hand show a much greater amplitude in change of $\mathrm{PA_{kin}}$.

It should be stressed again that determination of $\mathrm{PA_{kin}}$ for slow rotators is much more ill defined than for fast rotators in the sense that if there is no rotation, there is also no orientation of rotation. The abrupt changes in $\mathrm{PA_{kin}}$ are the consequence of this in some cases (NGC 4374, 4486, 4550, 5846), and while one could debate the robustness of measured $\mathrm{PA_{kin}}$, one should acknowledge the different nature of these systems from objects with a constant $\mathrm{PA_{kin}}$.

The difference between the slow and fast rotators is most visible in the amplitude of rotation. The middle panel of Fig. 3, shows the radial profiles of k_1 kinemetric terms for 48 early-type galaxies. Most of the profiles cover up to 1 R_e in radius. Slow-rotating galaxies can show a non-zero amplitude of rotation in the centres (KDCs), but the amplitude is, in general, not very high and towards the edge of the map it is mostly negligible. The only exception is NGC 5982, which approaches two fast rotators with the slowest rotation in the outer regions (NGC 4278 and 4473).

Another characteristic of this plot is the variety of profiles. They include: monotonically rising profiles (e.g. NGC 3032), profiles with an initial slow rise which turns to a more rapid one (e.g. NGC 524), a rapid rise to a maximum followed by a plateau (e.g. NGC 4546), rise to a maximum followed by a decrease (e.g. NGC 4526), double hump profiles (e.g. NGC 4660), flat profiles (e.g. NGC 821) and, in slow rotators, profiles showing a decrease below our detection limit. Keeping in mind that the SAURON sample is not a complete sample, among fast rotators there are 17 (47 per cent) with increasing profile at the edge of the SAURON map, nine (25 per cent) have flat profiles, five (14 per cent) decreasing profiles and four galaxies have intermediate (difficult to classify) profiles. Among slow rotators there are three (25 per cent) galaxies with increasing profiles at the edge of the map, the rest being flat and below the detection limit.

These statistics are influenced by the size of velocity maps and the coverage of kinematics components by kinemetric ellipses. Clearly, larger scale observations would detect the end of rise in amplitude in galaxies that are now observed to have increasing k_1. Similarly, it is possible that a decrease in k_1 could be followed by an additional increase or a flat profile at large radii. Still, there are two general conclusions for fast rotators: they mostly show increasing velocity profiles at 1 R_e, where the range of maximum velocity amplitude spans 200 km s^{-1}. On the other hand, slow rotators have velocity amplitude mostly less than 20 km s^{-1} at 1 R_e.

The bottom panel of Fig. 3 shows radial velocity dispersion profiles, σ_0, extracted along the isophotes from the velocity dispersion maps as a_0 harmonic terms. All profiles are normalized to their value at $R_e/5$. This highlights the similar general shape of the σ_0 radial profiles. The only outlier is NGC 4550 with an σ_0 profile which increases with radius. Most of the other profiles, while different in detail, show a general trend of increasing σ_0 towards the centre and also have a similar shape. A few profiles are consistent with being flat ($\Delta\sigma_0/\Delta R \lesssim 30$ km s^{-1}) over the whole profile (visible only in fast rotators such as NGC 7457).

If there are any real differences between σ_0 profiles, they are apparent for radii smaller than $R_e/5$. There are a few exceptions to the general trend: (i) profiles with a decrease of more than 5 per cent in the normalized σ_0 within $R_e/5$ (e.g. NGC 4382), (ii) profiles that are flat to within 5 per cent inside the $R_e/5$ (e.g. NGC 7457) and (iii) profiles with a central rise followed by a drop and consecutive rise forming a profile with double maxima (e.g. NGC 5813). These cases occur mostly in fast rotators, with a few exceptions in slow rotators.

These central plateaus and drops are interesting, because classical theoretical work predicts that, for constant mass-to-light ratio, $r^{1/n}$ light profiles have velocity dispersion minima in the centres of galaxies (Binney 1980; Ciotti & Lanzoni 1997), unless they contain central black holes (e.g. Merritt & Quinlan 1998). The central σ-drops evidently do not occur frequently in real early-type galaxies, but are, perhaps marginally more common to fast rotators. About 10 per cent of the SAURON early-types exhibit the central drop (but additional 20 per cent have flat central profiles), which is much less compared to 46 per cent among the Sa bulges, also observed with SAURON data (Falcón-Barroso et al. 2006).

4.3 Distribution of axial ratios

We now compare average photometric and kinematic axial ratios of SAURON galaxies. The axial ratio of a velocity map is related to the opening angle of the isovelocity contours. In other words, the pinching of the contours in a spider diagram is related to the axial ratio of the best-fitting ellipse given by kinemetry. As the kinematic axial ratio of slow rotators is an ill defined quantity (set to 1), in the rest of this section we focus on the average axial ratios of the fast rotators.

In Fig. 4 we compare values of $\langle q_{\rm kin}\rangle$ and $\langle q_{\rm phot}\rangle$ for fast-rotating galaxies. Since the typical seeing for SAURON data ranges up to 2.5 arcsec, we exclude the inner 5 arcsec of the $q_{\rm kin}$ profiles from our derivation of the luminosity-weighted average values (Appendix A). The left-hand panel shows a one-to-one correlation between the two quantities, although the scatter and uncertainties are large. The right-hand panel shows more clearly the amount of scatter in these relations, as measured by the difference $\langle q_{\rm kin}\rangle$ - $\langle q_{\rm phot}\rangle$. The typical variation of the measured average $\Delta q_{\rm kin}$ is 0.1, as shown with vertical guidelines on the right-hand panel. Outside this region there are about dozen galaxies. A few of these have $\langle q_{\rm kin}\rangle$ larger than $\langle q_{\rm phot}\rangle$; their photometric axial ratio is flatter than the kinematic, while the majority of outliers have the kinematic axial ratio flatter than the photometric. Let us consider in more detail only objects at significant distances from the vertical lines (i.e. $\langle q_{\rm kin}\rangle - \langle q_{\rm phot}\rangle > 0.15$): NGC 821, 4270, 4473, 4621, 5308 and 5838.

If we look at the $q_{\rm kin}$ profiles of the three galaxies (Fig. B1) with $\langle q_{\rm kin}\rangle > \langle q_{\rm phot}\rangle$, we can see that some of their kinematic subcomponents have axial ratios very similar to the local photometric axial ratios. Notably, in the case of NGC 5308 this is the outer component, especially at radii near to the edge of the SAURON FOV. The middle range, where the differences are the largest, is also the region of the transition between the two kinematic components. The mixing of the components changes the measured $\langle q_{\rm kin}\rangle$, but it should be also noted that the $\langle q_{\rm phot}\rangle$ varies over the whole map, becoming flatter and similar to $\langle q_{\rm kin}\rangle$ with radius. This is not the case in NGC 4473. Here the photometric axial ratio remains constant, but the kinematic axial ratio changes at larger radii. Again this change occurs in the transition region between the two kinematic components. Detailed dynamical modelling of this galaxy shows that it is made of two counterrotating stellar components of unequal mass. This object is physically similar to NGC 4550, where the main difference is in the mass fraction of the two components (Paper X). In the case of NGC 4270 it is the $q_{\rm phot}$ that steadily changes with radius, while $q_{\rm kin}$ has mostly high values, but shows abrupt changes between the points. These are related to sometimes rather high values of k_5/k_1, which also changes abruptly between the adjacent points, a behaviour originating from the noisy transition region between two kinematic components. Since it is hard to disentangle the noise from the genuine physical signal in $q_{\rm kin}$ measurement, and given the boxy appearance on the large scales, we note that this object could be a true and unusual outlier from the relation between $q_{\rm phot}$ and $q_{\rm kin}$.

Galaxies with $\langle q_{\rm kin}\rangle < \langle q_{\rm phot}\rangle$ are either single component (NGC 821 and 4621, if we exclude the CRC in NGC 4621 of $\sim$4 arcsec in size) or multi component (NGC 5838). The *HST* image of NGC 5838 has a prominent nuclear dust disc with the axial ratio

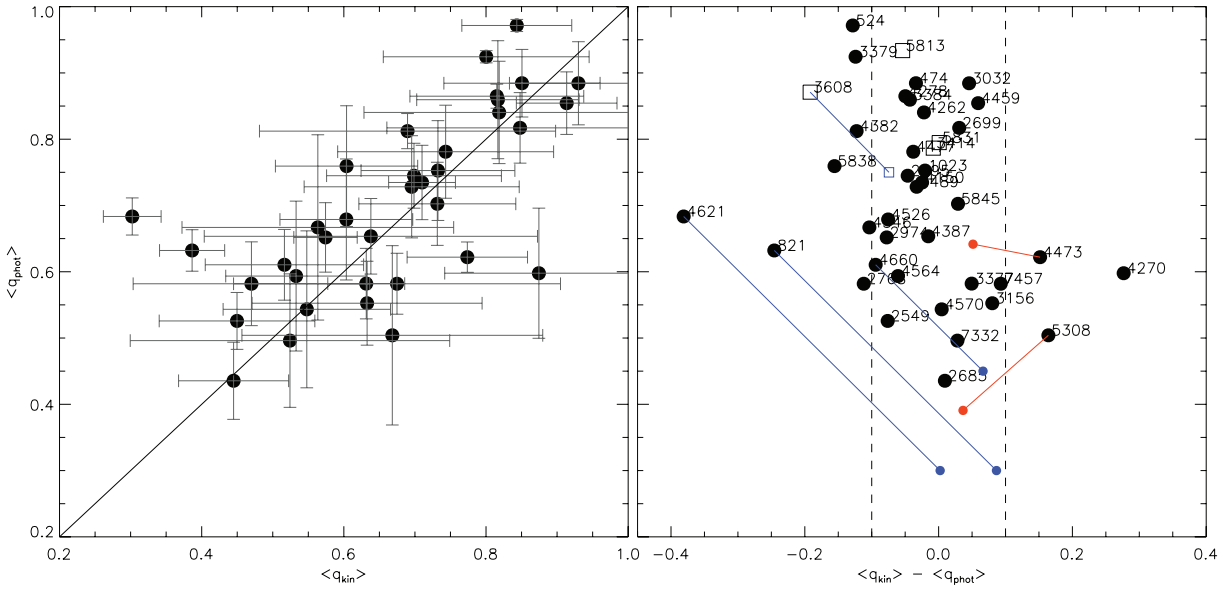

Figure 4. Left-hand panel: Relation between luminosity-weighted kinematic and photometric axial ratios, $\langle q_{\rm kin}\rangle$ and $\langle q_{\rm phot}\rangle$, respectively, for fast-rotating galaxies in the SAURON survey measured beyond 5 arcsec to avoid seeing effects. The black line is the 1:1 relation. The error bars describe the radial variations of $q_{\rm phot}$ and $q_{\rm kin}$ profiles. Right-hand panel: Difference between luminosity-weighted kinematic and photometric axial ratios plotted against the photometric axial ratio. Dashed vertical lines represent a typical variation of $q_{\rm kin}$ profiles, which is the dominant uncertainty factor for comparison with $q_{\rm phot}$. Solid symbols are fast-rotating galaxies, while open squares are KDC components of slow rotators. The red lines between symbols link $\langle q_{\rm kin}\rangle$ with $\langle q_{\rm phot}\rangle$ measured on inner (NGC 4473) and outer (NGC 5308) kinematic components. The blue lines link $\langle q_{\rm kin}\rangle$ and axial ratio of the MGE models.

between 0.3 and 0.4, constraining its inclination to about 70°. It is possible that the velocity map is dominated by the presence of an associated stellar disc embedded in the galaxy body. NGC 821 and 4621 were parametrized via the Multi-Gaussian Expansion (MGE) (Emsellem, Monnet & Bacon 1994; Cappellari 2002) in Paper IV. Both models required very flat Gaussians to reconstruct the light distribution (in both cases, the smallest axial ratios of the Gaussians of the MGE models were 0.3); these Gaussians are tracing discs embedded in spheroids. If we compare the $\langle q_{\rm kin}\rangle$ with the flattest MGE Gaussians, both galaxies move well within the two vertical lines on right-hand panel of Fig. 4 (blue lines).

As a matter of interest, on the same right-hand plot of Fig. 4 we overplotted axial ratios for the big KDCs in the sample: NGC 3414, 3608, 5813 and 5831. The shape of their kinematics is similar with the distribution of light, except in the case of NGC 3608. Its KDC has flatter kinematics than the light, but the flattest MGE Gaussian is comparable with the kinematic axial ratio. This suggests that even some of the subcomponents of the slow-rotating galaxies have similar properties like fast-rotating galaxies.

Having in mind that $q_{\rm kin}$ profiles can vary significantly with the radius, and the average values could be contaminated by the contribution of the transition regions between the components, we conclude that there is a near one-to-one correlation between average kinematic and photometric axial ratios in fast-rotating galaxies, with a number of objects having $\langle q_{\rm kin}\rangle < \langle q_{\rm phot}\rangle$, and, hence, having disc-like components more visible in their kinematics than in photometry.

4.4 Shape differences between velocity dispersion and surface brightness maps

As shown in Section 3.2, the isophotes are not necessary a good representation of contours of constant velocity dispersion and the deviations are visible in the second cosine term (b_2) of the harmonic decomposition of the velocity dispersion profiles extracted along the isophotes. In Fig. 5 we quantify the differences between isophotes and iso-σ contours by plotting the normalized luminosity-weighted second term ($\langle b_2/a_0\rangle_\sigma$) extracted along the isophotes of SAURON galaxies. Slow rotators are shown in red.

Focusing on the left-hand panel, it is clear that galaxies in the sample span a large range of $\langle b_2/a_0\rangle_\sigma$, both positive and negative. If we exclude NGC 4473 and 4550, there is a tail of galaxies with negative values up to ~ -0.1. Also, it seems that there is a trend of high negative $\langle b_2/a_0\rangle_\sigma$ in flat galaxies: as galaxies become rounder, $\langle b_2/a_0\rangle_\sigma$ tends to zero; above $\langle q_{\rm phot}\rangle = 0.8$ galaxies have small absolute value of $\langle b_2/a_0\rangle_\sigma$. Slow rotators are relatively round systems (Paper X) with $q_{\rm phot} > 0.7$ (excluding the special case of NGC 4550). Their $\langle b_2/a_0\rangle_\sigma$ values are small and mostly positive. Typical measurement error of $\langle b_2/a_0\rangle_\sigma$ is ∼0.03, and hence, the slow rotators are consistent with having velocity dispersion maps very similar to the distribution of light, with possibly marginally flatter iso-σ contours.

Before we turn to the right-hand panel in Fig. 5, let us go back to Fig. 1 and the example of NGC 2549 and 4473. Their stellar velocity dispersion maps have different shapes from the distributions of light, but they have similar absolute values of $\langle b_2/a_0\rangle_\sigma$; they fall on the opposite sides of Fig. 5. There is, however, evidence that in both cases the deviations from the photometry have similar physical origin. NGC 2549 shows clear photometric and kinematic evidence for a stellar disc viewed at a high inclination (Fig. B1). The velocity dispersion map has a very specific 'bow-tie' shape in the central 10 arcsec, while outside its amplitude is low everywhere. The 'bow-tie' shape can be explained with a light-dominating dynamically cold stellar disc which decreases the observed velocity dispersion. Outside of the disc, the bulge dominates and the observed velocity dispersion is again higher. It should be noted that the view of the galaxy at a high inclination is crucial for this effect to be seen.

NGC 4473 was discussed in the previous section where we stated that it actually contains two subcomponents. One of them is flat and counterrotates with respect to the main galaxy body. This can

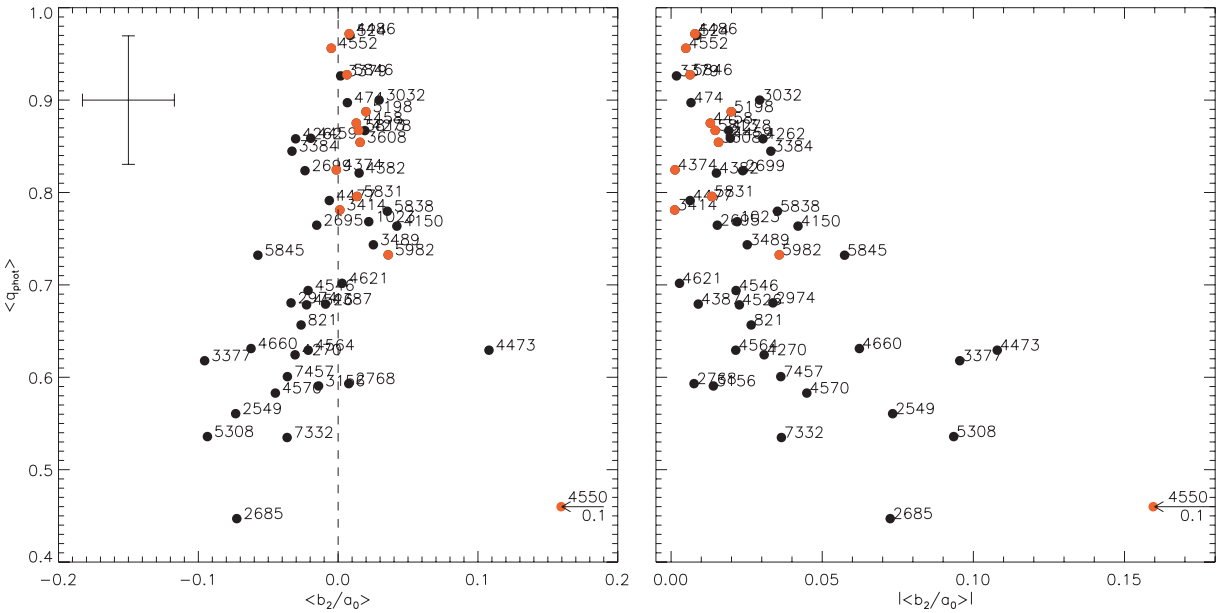

Figure 5. Left-hand panel: Relation between isophotal axial ratio and the luminosity-weighted average normalized second term ($\langle b_2/a_0\rangle_\sigma$) of the Fourier decomposition of the velocity dispersion profiles extracted along the isophotes. Red symbols are slow rotators. An average uncertainty, describing the radial variation of b_2/a_0 profiles, is shown in the upper left-hand corner. Large negative $\langle b_2/a_0\rangle_\sigma$ values are typical for iso-σ contours that are rounder than the isophotes, while large positive $\langle b_2/a_0\rangle_\sigma$ values are typical for flatter iso-σ contours than the isophotes. Right-hand panel: Same as left-hand panel, but now absolute values of $\langle b_2/a_0\rangle_\sigma$ are plotted. In both images, NGC 4550 was shifted to the left-hand side for 0.1 for presentation purposes, as shown by the arrows.

explain the rise of the velocity dispersion along the major axis, specifically at larger radii where the contribution of the flat component becomes similar to the main body. This is also visible in the mean velocity map, where beyond 10 arcsec the velocity starts dropping. The only significant difference between these two examples is in the sense of rotation of the flat subcomponents. Corotating discs or flattened components, viewed at favourable angles will likely show negative $\langle b_2/a_0\rangle_\sigma$, while counterrotating components will contribute to positive $\langle b_2/a_0\rangle_\sigma$. In other words, corotation increases, while counterrotation decreases the flattening of the iso-σ contours.

A similar case is NGC 4550, the most extreme outlier, which also has two counterrotating discs. NGC 4150 and 3032 can be put in the same group: the OASIS measurements resolve their CRC components. It is interesting to note that the strongest σ-drop galaxies (NGC 2768 and 4382) are both found on the positive side of the left-hand panel of Fig. 5, admittedly with small $\langle b_2/a_0\rangle_\sigma (<0.02)$, indicating that the shapes of the velocity dispersion maps of σ-drop objects are somewhat different from the shapes of galaxies with central plateaus in velocity dispersion profiles or bow-tie shape of velocity dispersion maps. The shapes of σ-drops are more similar to the isophotes than the shape of iso-σ contours in the objects with strong near to edge-on discs such as NGC 2549 or 3377. If σ-drops, bow-ties and central plateaus are all caused by discs, than the difference between them might originate from the orientation of the galaxy, where bow-ties are seen at edge-on and σ-drops at face-on orientations.

Given the uncertainties, it is hard to argue either way about other galaxies with slightly positive $\langle b_2/a_0\rangle_\sigma$ values. Other effects, such as the actual size of the components or the presence of dust, may play a role on that level. This should be noted, but we, however, continue by suggesting that the main contributors to the shape difference between the zeroth and the second moment of the LOSVD in early-type galaxies are the embedded discs or flattened fast-rotating components seen at different inclination. In this respect, on the right-hand panel of Fig. 5 we plot the absolute value of $\langle b_2/a_0\rangle_\sigma$. Here a trend is clear: from round slow rotators with generally small absolute values to flat fast-rotating galaxies with increasing $|\langle b_2/a_0\rangle_\sigma|$. This sequence is the one of increasing contribution of the ordered rotation towards the total energy budget, but it is, unfortunately, dependent on the viewing angles (NGC 524 with the face-on disc in the top left-hand corner of the diagram) and on the luminosity-weighted contribution of the flat component to the total kinematics (CRC in NGC 4621 is not detected).

4.5 Higher order moments of the LOSVD

The final part of our analysis of the kinematic moments of the LOSVD is devoted to maps of h_3 and h_4, the Gauss–Hermite moments which measure deviations of the LOSVD from a pure Gaussian. They were introduced because LOSVD profiles are rather non-Gaussian, specifically the contribution of h_3, the skewness, along the major axis of galaxies was found to have large amplitudes (e.g. van der Marel et al. 1994). In a diagram of local h_3– V/σ relation, Bender et al. (1994) plotted the major axis points of their objects which could be separated in two distinct groups made of galaxies with discy isophotes and non-discy isophotes. Both groups showed anticorrelation between h_3 and V/σ, where the points with small V/σ values in the centre of the diagram had a steeper slope. It was recognized that the discy early-type galaxies cover a large range in V/σ and are responsible for tails in upper left-hand and lower right-hand corner of the diagram, while non-discy early-types with small V/σ values showed a somewhat smaller range in h_3 values.

On the top panel of Fig. 6 we plot the local h_3– V/σ relation for all data points of 48 SAURON galaxies. Red points belong to Voronoi bins of the slow rotators. This plot is somewhat different from previous findings. Paper X showed that slow rotators have

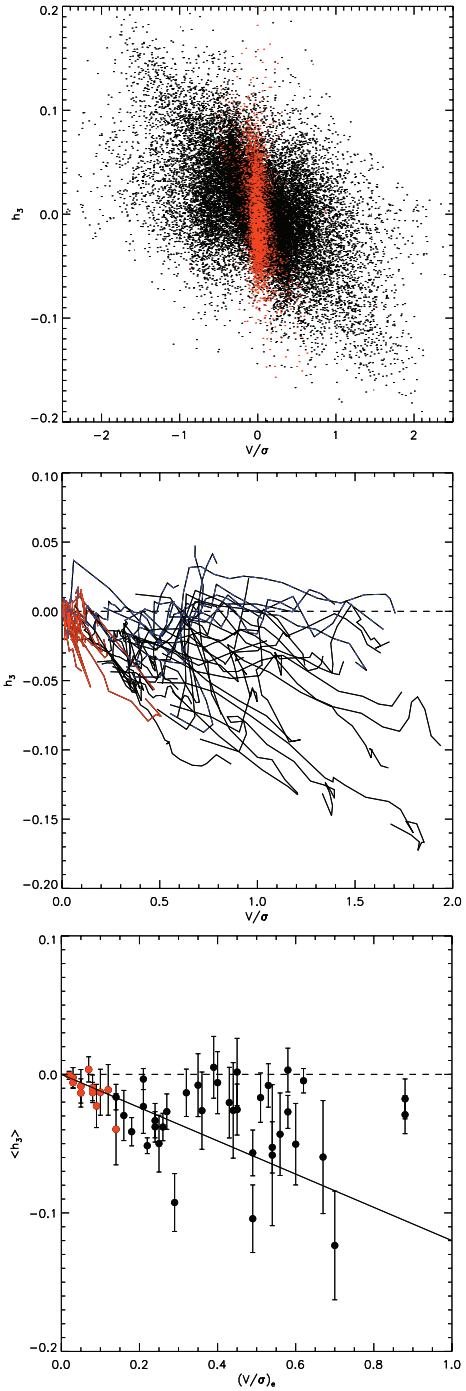

Figure 6. Top: Local h_3– V/σ relation for all data points of the 48 SAURON galaxies with h_3 error less than 0.2. Middle: Profiles of h_3– V/σ relation averaged on ellipses. On all maps (V, σ and h_3) profiles were extracted along the best-fitting ellipses to the velocity maps. Typical error bars are of the order of 0.01 or smaller, due to averaging along the best-fitting ellipse. Bottom: Relation between the luminosity averaged h_3 and $(V/\sigma)_e$(V/σ within 1 R_e from Paper X). The error bars describe the radial variation of h_3 profiles. The solid line is the relation from Bender et al. (1994). In all panels, slow rotators are shown in red.

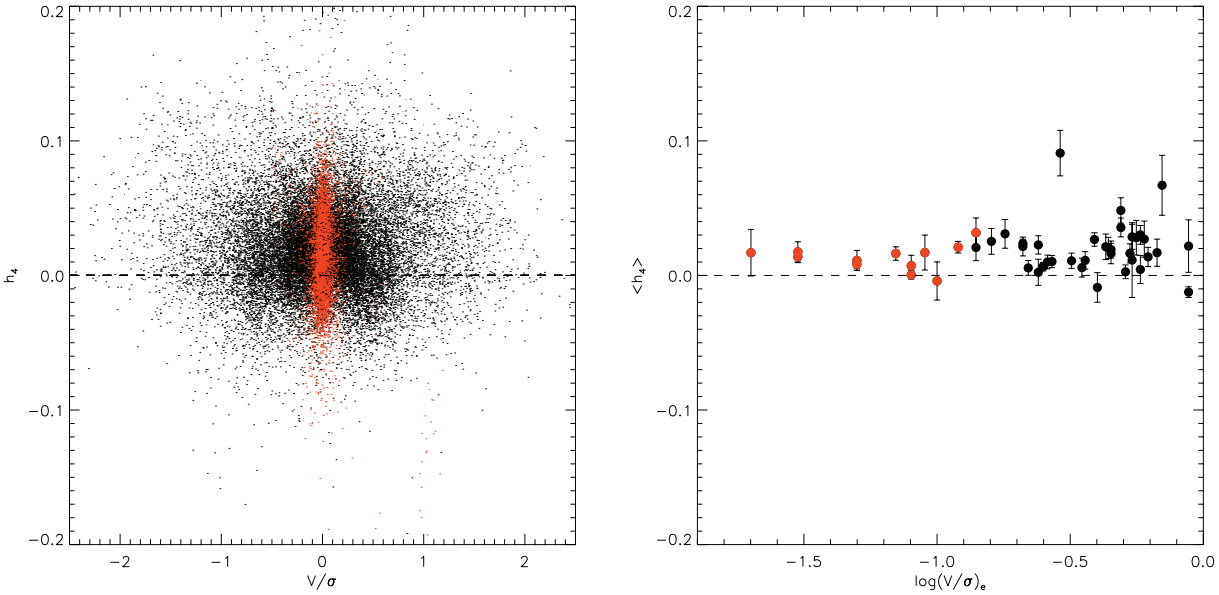

Figure 7. Left-hand panel: Local correlation between h_4 and V/σ for all data points of the 48 SAURON galaxies with h_4 error less than 0.2. Right-hand panel: Correlation between luminosity-weighted values average $\langle h_4 \rangle$ and $(V/\sigma)_e$ (Paper X). Red symbols are slow rotators in both panels. The error bars describe the radial variation of h_4 profiles.

small global V/σ and this is also reflected in bin-by-bin values. The black points represent the Voronoi bins of fast rotators, and their distribution is different from what was found before for discy ellipticals. The shape of the distribution of black points can be described as a superposition of two components: one which is anticorrelated with V/σ and makes distinct tails in upper left-hand and lower right-hand corner of the diagram (large positive and negative V/σ values), and the other that is both consistent with $h_3 \sim 0$, and shows positive correlation at intermediate V/σ.

Existence of $h_3 \sim 0$ distribution of points could be explained by the fact that, while Bender et al. (1994) plot only the points along the major axis, we plot them all, and the horizontal distribution and correlating tails are the consequence of the minor axis contamination. Using kinemetry we extracted profiles of the dominant harmonic terms from V, σ and h_3 maps along the same best-fitting ellipses to the velocity maps.[3] We plot the h_3– V/σ profiles on the middle panel of Fig. 6. These profiles are basically major axis representation of two-dimensional maps and are more comparable with previous major axis data. The slow rotators (in red) have the smallest V/σ values and generally small amplitudes of h_3. The two trends for fast rotators from the left-hand panel are still visible. Fast rotators cover a range of V/σ values, but some have large and some small h_3 amplitudes for a large V/σ values. In some specific cases there is a suggestion that h_3 changes the sign becoming positive and correlating with V/σ (e.g. NGC 5308) at larger radii.

A confirmation of this can also be seen on the bottom panel of Fig. 6. Here we plot the relation between luminosity averaged h_3 and $(V/\sigma)_e$ obtained within 1 R_e, as advocated by Binney (2005, values taken from Paper X). The shown error bars are not statistical uncertainties but describe the radial variation of h_3 profiles. This plot can be compared to fig. 14b of Bender et al. (1994), which also shows galaxies with $\langle h_3 \rangle \sim 0$ for intermediate V/σ_m, while their empirical fitting relation (the solid line) describes the general trend in our data.

The last kinematic moment to be analysed is given by the h_4 Gauss–Hermite coefficient. This moment describes the symmetric departures of the LOSVD from a Gaussian. It should be, however, kept in mind that it is very difficult to measure h_4 robustly, since it strongly depends on the effect of template mismatch. Also an inaccurate removal of the continuum will cause spurious h_4 values.

On the left-hand panel of Fig. 7 we plot the local h_4– V/σ relation. Slow rotators with small V/σ values, dominate the central region. They cover a range of positive h_4 values and somewhat extend below zero. Fast rotators fill in a cloud around slow rotators, equally filling negative and positive V/σ part of the plot. There is a suggestion for a larger spread in V/σ for positive h_4 values. Luminosity-weighted average $\langle h_4 \rangle$ values extracted with kinemetry along the isophotes are presented as a function of luminosity-weighted V/σ measured within 1 R_e (Paper X) in right-hand panel of Fig. 7. As $(V/\sigma)_e$ increases, there is a marginal trend of an increased spread in the observed h_4 values, and galaxies with negative average values start to appear. This result is similar to Bender et al. (1994), in the sense that negative $\langle h_4 \rangle$ appear for larger $(V/\sigma)_e$, but we do not find as negative values of $\langle h_4 \rangle$. The only slow rotator with negative $\langle h_4 \rangle$, however, is the usual outlier, NGC 4550, the special case of two counterrotating discs.

5 DISCUSSION

5.1 Velocity maps of slow and fast rotators

Radial profiles of kinemetric coefficients show that early-type galaxies are (i) multicomponent systems and (ii) in the majority of the cases contain a kinematic equivalent of a disc-like component. These statements are based on the empirical verification that the assumption of kinemetry holds. The assumption is that the azimuthal

[3]Note that here we rerun kinemetry on σ maps along the best-fitting ellipses for velocity maps, except in the case of the slow rotators when we used circles as explained in Section 3.2. These profiles are somewhat different from the profiles presented in Section 4.4 which were obtained along the isophotes.

profiles, extracted from a velocity map along the best-fitting ellipses, can be described with a simple cosine variation. Practically, this means that higher order harmonic terms are negligible and at our resolution we find that the deviation from the pure cosine law is less than 2 per cent, for about 80 per cent of cases, at least on a part of the map. The multiple components are visible in the abrupt and localized changes of kinemetric coefficients. The central regions often harbour separate kinematic components which corotate or counterrotate with respect to the outer body. In some cases there are more than two components (e.g. NGC 4382) or components are similar in size and cospatial (e.g. NGC 4473). Although the axial ratio profile in edge-on systems can change with the seeing effects (see Appendix A), and in some cases the seeing can alter the map considerably, the kinematic subcomponents are usually robust features.

There are, however, early-type galaxies for which the deviations from the cosine law exceed 10 per cent across a significant radial range. Such objects are all classified as slow rotators in Paper IX. The breakdown of the kinemetry assumptions is another evidence that these objects are intrinsically different. Certainly, we might not be able to apply kinemetry a priori in its odd version on velocity maps that do not show odd parity (e.g. NGC 4486), but in the case of slow rotators that show a detectable level of rotation (e.g. NGC 5982), the kinemetric analysis clearly shows differences from the maps of fast rotators (e.g. NGC 4387).

There are three types of intrinsic structures that will show small mean velocities: (i) face-on discs, (ii) two counterrotating equal in mass and cospatial components and (iii) triaxial structures.

(i) Face-on discs: Low inclination thin discs will still have minimal deviations from the cosine law assumed in kinemetry. Although the amplitude of the rotation in such cases is small, the disc-like rotation (negligible k_5/k_1 coefficients) is expected at all projections except in the actual case of $i = 0^\circ$ with no rotation. Such an example in the sample is NGC 524 ($i \sim 19^\circ$). Based only on the velocity map, one could naively interpret that NGC 4486 is a thin disc at $i = 0^\circ$, given that it has $q_{\rm kin} \sim 1$ and shows no rotation. However, other moments of the LOSVD strongly rule out this geometry, while, in general, other slow rotators are not round enough to even be considered as such extreme cases.

(ii) Counterrotating components: This case can be outlined with NGC 4550 and 4473. These galaxies are examples of axisymmetric objects with two counterrotating and cospatial components. The first one is classified as a slow rotator, while the other one is a fast rotator. In both cases, however, it is the mass fraction of the components that really decides what is observed. In the case of NGC 4550 the masses are nearly equal and the luminosity-weighted mean velocity is almost zero in the central region. NGC 4550 is a product of a very specific formation process, but a clear example of how a superposition of two fast-rotating components can imitate a slow rotator. In NGC 4473, on the other hand, one component is more massive and dominates the light in the central 10 arcsec, where the rotation is clearly disc like. Outside this region, where the counterrotating component starts to significantly contribute to the total light, the shape of the velocity map changes, the amplitude of the rotation drops and non-zero k_5/k_1 coefficients are necessary to describe stellar motions.

(iii) Triaxial objects: Observationally, these objects are marked by kinematic twists and kinematic misalignments, which are not present in axisymmetric galaxies. A strong restriction to the shape of the velocity maps of axisymmetric galaxies is that they should not have a radial variation of $\rm PA_{kin}$ or a misalignment between kinematic and photometric position angles. This, however, is not the case for triaxial galaxies, where the change of position angle can be influenced by a true change of the angular momentum vector, by the orientation of the viewing angles or by the relative dominance of different orbital families (Franx, Illingworth & de Zeeuw 1991; Statler 1991; van den Bosch et al. 2008). Paper X found that, globally, kinematic misalignments are present only in slow-rotating galaxies. Locally, however, we find both kinematic misalignments and twists in some fast-rotating objects as well, but they are mostly confined to central components or clearly related to bars (e.g. NGC 1023) or galaxies with shells (e.g. NGC 474).

We do not find strong kinematic twists typical of the extreme cases of maximum entropy models of triaxial galaxies projected at various viewing angles (Statler 1991; see also Arnold, de Zeeuw & Hunter 1994) for velocity maps of Stäckel triaxial models). Given that our sample is not representative of the luminosity function of local early-type galaxies in the sense that it contains too many massive galaxies, which are also more likely to show extreme features on the velocity maps, it is remarkable that we find that only a few velocity maps are similar to those predicted. Still, the observed velocity maps are divers (e.g. the difference between the maps of slow and fast rotators) and their complexity reflects the difference in their internal structure.

The profiles of the relative change of the kinematic position angles from the first panel of Fig. 3 suggest that fast and slow rotators have genuinely different intrinsic shapes, fast rotators being mostly axisymmetric and slow rotators weakly triaxial. This is also reflected in k_5/k_1 ratio. We suggest that the high values of this ratio in slow rotators, which is in practice caused by the noise in non-rotating velocity maps, has its origin in the internal orbital make up of these galaxies. Weakly triaxial slow rotators contain box orbits, and competing contributions of different tube orbit families, as opposed to more axisymmetric fast rotators with short-axis tubes as the only major orbit family (de Zeeuw 1985).[4] This suggestion is also supported by the analysis of the orbital structure of collisionless merger remnants (Jesseit, Naab & Burkert 2005) as well as by the kinemetric analysis of velocity maps of simulated binary disc merger remnants (Jesseit et al. 2007).

5.2 Evidence for discs in fast rotators

Kinematic subcomponents with azimuthal profiles that can be fitted with a cosine law are described as having a *disc-like rotation* (DR). This does not mean that they are actual discs. It just suggests that velocity profiles of early-type galaxies extracted along the best-fitting ellipse *resemble* the velocity maps of thin discs in circular motion. The rate of occurrence of DRs is, however, striking. There is no reason why this should be the case in early-type galaxies, which in principle as a class can have a triaxial symmetry and complex motion in different planes. As suggested above, the link between the kinemetry assumption and the structure of fast-rotating galaxies has its origin in their internal structure.

The results of the dynamical models in Paper X reveal that fast rotators show evidence for a kinematically distinct flattened spheroidal component, suggesting that fast rotators are nearly oblate and contain flattened components. In addition to these dynamically cold components, the stellar populations of fast rotators show evidence

[4]We should keep in mind that two short-axis tube families with opposite angular momentum in certain cases can produce axisymmetric objects which appear as slow rotators, as mentioned above in the case of NGC 4550.

for different chemical components. Kuntschner et al. (2006) find that all morphologically flat fast rotators have Mg b line-strength distribution flatter than the isophotes, and associate it with the rotationally supported substructure, which features a higher metallicity and/or an increased Mg/Fe ratio as compared to the galaxy as a whole.

These are some of the dynamical and chemical evidences for disc-like components in fast rotators. What is the kinemetric evidence? As mentioned above, we find that velocity maps of fast rotators are mostly described by a simple cosine law, as are velocity maps of thin discs. We also find an almost one-to-one correspondence between the projected shape of the stellar distribution and the shape of the observed kinematic structure in fast-rotating galaxies. The connection between the shape and the kinematics is supported by an assumption that rotation influences the shape of the object by flattening it and, for isotropic models, the rotation speed responsible for flattening of the shape is related to the shape of the stellar distribution as $\sim \sqrt{\epsilon}$ (Binney & Tremaine 2008, section 4.8.2). In order to investigate further the $\langle q_{\rm phot}\rangle - \langle q_{\rm kin}\rangle$ correlation we constructed two-integral analytic models of early-type galaxies.

The isotropic models we used were previously presented in appendix B of Paper X, to which we refer the reader for more details. The main point of these Jeans models is that we used as templates 6 galaxies, which represent some of the typical types from the SAURON sample. Their light distribution was parametrized in Paper IV by the MGE method, and was used as the basis for the intrinsic density distributions. Observables of each Jeans model were projected at six different inclinations: 90°, 80°, 65°, 50°, 35° and 25°. These models are not meant to reproduce the observed kinematics in detail, but they are self-consistent, and under the assumption of axisymmetry and isotropy, they predict velocity maps and offer an opportunity to study the relation between the shape and kinematics.

On the left-hand panel of Fig. 8 we show the difference between the luminosity-weighted average values of $\langle q_{\rm kin}\rangle$ and $\langle q_{\rm phot}\rangle$, measured by kinemetry on the model images and velocity maps, in the same way as for the SAURON data in Fig. 4 (also excluding the inner 5 arcsec). Different colours represent Jeans models based on different template galaxies. Each symbol corresponds to a model at different inclination, where the points move from top to bottom with increasing inclination (from 25–90°). It is clear that for small inclination $\langle q_{\rm kin}\rangle \approx \langle q_{\rm phot}\rangle$, but as the models are viewed closer to edge-on there is a trend of increasing differences between the axial ratios and in some cases a trend of larger variation along the profiles represented by larger error bars for progressively more inclined models. Specifically, in all but one marginal case $\langle q_{\rm kin}\rangle > \langle q_{\rm phot}\rangle$: in these models velocity maps are 'rounder' than images. The velocity map of the Jeans model of NGC 4621, whose MGE parametrization has the flattest Gaussian, has a flat component along the major axis, which becomes more prominent with increasing inclination, contributing to the radial variation and increasing $q_{\rm kin}$ with respect to $q_{\rm phot}$. The kinematics of this component is the most 'disc-like' in our Jeans models with tightly pinched isovelocity contours. For comparison, the model for NGC 3377 also has a similar thin MGE component. This component contributes to the disc-like kinematic component confined to the central region, but since it is not as prominent in the total light, such as the one in the NGC 4621 MGE model, only traces of the disc-like component can be seen in both photometry and kinematics.

The contrast between observed galaxies and isotropic models is significant. The isotropic models predict $\langle q_{\rm kin}\rangle \geq \langle q_{\rm phot}\rangle$ for $i \gtrsim 30°$, but the models also show that prominent disc-like photometric features will generate pinched isovelocity contours and decrease $\langle q_{\rm kin}\rangle$ pushing the galaxies towards the observed trend of, on average, $\langle q_{\rm kin}\rangle \sim \langle q_{\rm phot}\rangle$ or even $\langle q_{\rm kin}\rangle < \langle q_{\rm phot}\rangle$. It seems reasonable to assume that while isotropic models can explain certain features of

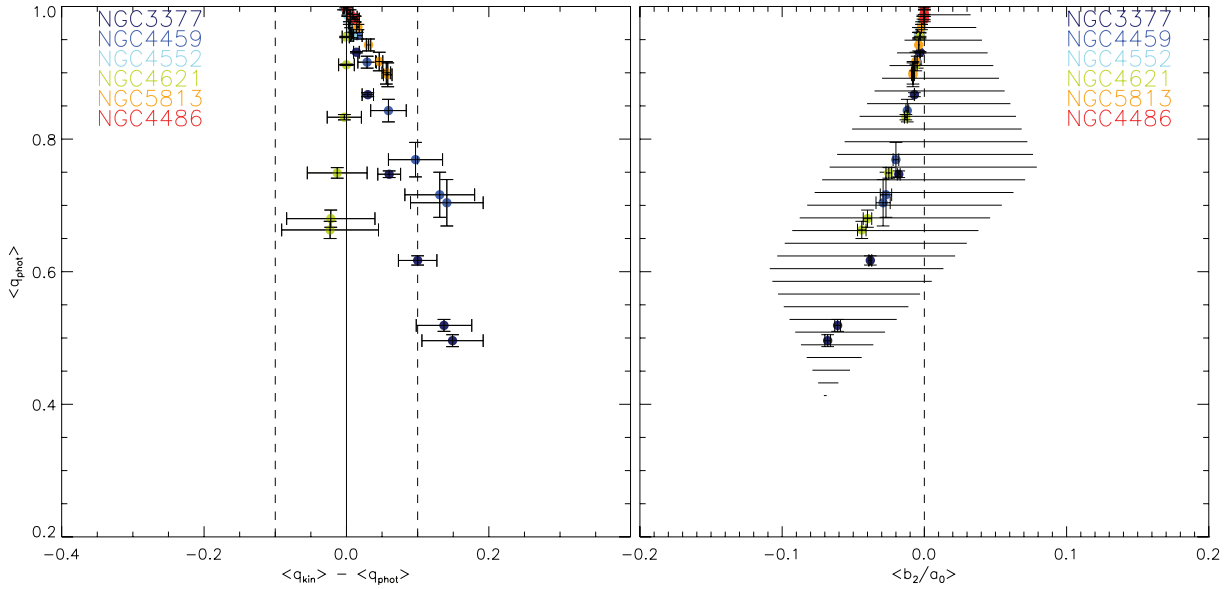

Figure 8. Left-hand panel: Difference between luminosity-weighted kinematic and photometric axial ratio, $\langle q_{\rm kin}\rangle$ and $\langle q_{\rm phot}\rangle$, for five Jeans models at 25°, 35°, 50°, 65°, 80° and 90° inclinations plotted against the luminosity-weighted photometric axial ratio. The increase in inclination decreases $\langle q_{\rm phot}\rangle$ and moves points downwards. The vertical dashed lines are guidelines of the variation of $q_{\rm kin}$ profiles from the SAURON data as in Fig. 4. Vertical solid line shows the location of zero difference between $\langle q_{\rm phot}\rangle$ and $\langle q_{\rm kin}\rangle$. Right-hand panel: Relation between photometric axial ratio and absolute $\langle b_2/a_0\rangle_\sigma$ for the same Jeans models as on the left-hand panel. With increasing inclination the points move towards more negative $\langle b_2/a_0\rangle_\sigma$ values. The hatched area represents the location of the data from Fig. 5.

fast rotators, they cannot describe them as a class of galaxies. It is the embedded flattened components, often visible only in the kinematics that are responsible for the observed differences between the models and the data.

This can be also seen by comparing the difference in shape between the isophotes and iso-σ contours (Fig. 5). We repeated the same exercise with velocity dispersion maps of our isotropic Jeans models. Results are shown on the right-hand panel of Fig. 8. The trend shown here of a larger absolute $\langle b_2/a_0\rangle_\sigma$ values with lower $\langle q_{\rm phot}\rangle$ is very similar to the observed trend (hatched region). The test can also explain the shape of the observed trend: large absolute values of $\langle b_2/a_0\rangle_\sigma$ can be observed when the object contains a significant flattened component and it is observed at larger inclinations. The most affected are again NGC 4621 and 3377 models. As before, the isotropic models are able to explain part of the observed data, but not the details of the distribution. Specifically, the shape of the iso-σ contours of slow rotators ($\langle b_2/a_0\rangle_\sigma > 0$) is not reproduced well by the isotropic models. Similarly, the spread in $\langle b_2/a_0\rangle_\sigma$ of fast rotators is also not well reproduced. Clearly, our Jeans models are much simpler than the real galaxies, lacking by construction multiple kinematic and especially counterrotating components. Comparing the kinemetric analysis of the Jeans models and the observed objects, we find that fast-rotating galaxies are more complex than isotropic rotators, presumably containing also flattened kinematically distinct components, which can corotate or counterrotate on top of the non-rotating or isotropically rotating spheroid.

The evidence for discs in fast rotators are also present in the ratio of h_3 and V/σ. h_3 measures the asymmetric deviations from the Gaussian LOSVD and the anticorrelation of h_3 with V/σ is taken to show presence of discs. Our results confirm previous findings that early-type galaxies on the whole have asymmetric LOSVDs, but this applies only to fast rotators. We also find that many fast rotators show constant and close to zero h_3 profiles, or, in a few cases, show a change from negative to positive values with increasing radius, similar to what is seen in peanut bulges and bars (Chung & Bureau 2004; Bureau & Athanassoula 2005).

The embedded flattened components in fast rotators are also evident when h_3– V/σ diagram is compared with the results of merger simulations (Balcells 1991; Bendo & Barnes 2000; Naab & Burkert 2001; González-García et al. 2006). Specifically, the updated h_3–V/σ diagram in Fig. 6 can be compared with fig. 16 from Naab et al. (2006), who discuss the influence of dissipational mergers in which embedded discs are formed in merger remnants. Our figure compares rather well with a combination of 1:1 dry and 1:3 wet mergers. This comparison suggest that it is not possible to explain the LOSVD of early-type galaxies with one merging track only, but that slow rotators predominantly originate in major colissionless mergers, while fast rotators are remnants of dissipational mergers.

The comparison of our bin-by-bin h_4– V/σ diagram (right-hand panel in Fig. 7) and lower four panels of fig. 16 in Naab et al. (2006) is equally impressive, although their simulations predict somewhat too negative values of h_4. Again, the observations are largely consistent with the scenario where slow rotators originate from dry 1:1 mergers, while fast rotators from a combination of dry and wet 1:3 mergers.

Combining all the evidence presented in the previous section, we suggest that fast rotators are dominated by discs (e.g. NGC 3156, 2685). When their light is dominated by the bulge, their kinematics still show strong disc components (e.g. NGC 821, 4660). In either case, *fast rotators contain flattened fast-rotating components and this dynamical property differentiates them from slow rotators*. We suggest that with increasing specific angular momentum, $\lambda_{\rm R}$, the relative mass of the embedded discs also increases and contributes more significantly to the total mass. Among the disc-like components in fast rotators there is a range of flattenings reflecting a diversity in possible formation paths which create, preserve and/or thicken discs within spheroids, such as passive fading of spirals and multiple minor dissipational mergers. The change within the internal structure is observationally reflected in the transition between slow and fast rotators, which offers possible anchor points for theoretical models of galaxy evolution.

6 CONCLUSIONS

Using kinemetry we analysed two-dimensional maps of 48 early-type galaxies observed with SAURON and velocity maps of a subsample observed with OASIS. The analysed maps are: reconstructed image, mean velocity, velocity dispersion, h_3 and h_4 Gauss–Hermite moments. The reconstructed images and the maps of the mean velocity were analysed along the best-fitting ellipses. Maps of the higher moments of the LOSVD were analysed either along the isophotes (velocity dispersion, h_4) or best-fitting ellipses from velocity maps (h_3). We presented the profiles of kinemetric coefficients for velocity maps, being the dominant kinematic moment of the LOSVD and having the highest signal-to-nose ratio.

Kinemetry and its kinemetric coefficients allow us (i) to differentiate between slow and fast rotators from velocity maps only and (ii) to indicate that fast-rotating galaxies contain discs with a larger range in the mass fractions to the main body. The results of this paper can be summarized as follows.

(i) Following the kinemetric analysis of the velocity maps it is possible to distinguish between galaxies with *single* and *multiple components*. Components can be described as having a *disc-like rotation*, *low-level velocity*, *kinematic misalignment*, *kinematic twist* or being *kinematically decoupled component*. The sorting of galaxies in these groups is based on kinemetric coefficients: $\rm PA_{kin}$, $q_{\rm kin}$, k_1 and k_5/k_1.

(ii) The majority of early-type galaxies are MC systems (69 per cent).

(iii) The total fraction of galaxies with a DR component (including all that have $k_5/k_1 < 0.02$) is 81 per cent. In terms of S0/E classification, 92 per cent of S0s and 74 per cent of Es have components with disc-like kinematics.

(iv) KDCs are found in 29 per cent of galaxies. These KDC are of different sizes, some are not resolved at SAURON resolution and appear as CLVs, but are clearly detectable in the OASIS observations at higher spatial resolution.

(v) Early-type galaxies with constant $\rm PA_{kin}$(ΔPA $< 10^\circ$ outside any central component) are fast rotators. All fast rotators have a DR component.

(vi) Most fast rotators have $\langle q_{\rm kin}\rangle \lesssim \langle q_{\rm phot}\rangle$. Their kinematics often shows a structure flatter than the distribution of light. This means that images alone are not sufficient to recognize all fast rotators (e.g. NGC 524 or NGC 3379 would be missed).

(vii) In face-on galaxies, isophotes are coincident with iso-σ contours. In edge-on galaxies, however, there are differences which can be detected with kinemetry. Specifically, the edge-on fast rotators contain dynamically cold components which changes the shape of iso-σ contours.

(viii) Slow-rotating galaxies have low V/σ and a range in h_3 amplitudes. Fast-rotating galaxies have large spread in h_3 which anticorrelates with V/σ. There is, however, a significant number of

fast-rotating galaxies which have h_3 radial profiles that change from strongly negative to near to zero h_3 values. Similar behaviour was found in bar galaxies or in remnants of colissionless mergers.

(ix) Allowing for large uncertainties in the determination of h_4, our data show a trend where slow and fast rotators have similar h_4 values, with a weak tendency for an increased spread of h_4 in fast rotators, also dependant on V/σ. These trends can be explained through a combination of dry and wet mergers of both equal and unequal in mass progenitors.

(x) Dissimilarities between slow and fast rotators originate in their different internal structures. Slow rotators are mildly triaxial objects supporting a variety of orbital families. Fast rotators are axisymmetric spheroids with embedded flattened components of different mass fraction ranging from completely disc dominated systems to small central discs visible only in kinematics.

ACKNOWLEDGMENTS

DK acknowledges the support from Queen's College Oxford and hospitality of Centre for Astrophysics Research at the University of Hartfordshire. The SAURON project is made possible through grants 614.13.003, 781.74.203, 614.000.301 and 614.031.015 from NWO and financial contributions from the Institüt National des Sciences de l'Univers, the Université Lyon I, the Universities of Durham, Leiden and Oxford, the Programme National Galaxies, the British Council, PPARC grant 'Observational Astrophysics at Oxford 2002–2006' and support from Christ Church Oxford, and the Netherlands Research School for Astronomy NOVA. RLD is grateful for the award of a PPARC Senior Fellowship (PPA/Y/S/1999/00854) and postdoctoral support through PPARC grant PPA/G/S/2000/00729. The PPARC Visitors grant (PPA/V/S/2002/00553) to Oxford also supported this paper. GvdV acknowledges support provided by NASA through grant NNG04GL47G and through Hubble Fellowship grant HST-HF-01202.01-A awarded by the Space Telescope Science Institute, which is operated by the Association of Universities for Research in Astronomy, Inc., for NASA, under contract NAS 5-26555. JFB acknowledges support from the Euro3D Research Training Network, funded by the EC under contract HPRN-CT-2002-00305. This paper is based on observations obtained at the William Herschel Telescope, operated by the Isaac Newton Group in the Spanish Observatorio del Roque de los Muchachos of the Instituto de Astrofísica de Canarias. Based on observations obtained at the Canada–France–Hawaii Telescope (CFHT) which is operated by the National Research Council of Canada, the Institut National des Sciences de l'Univers of the Centre National de la Recherche Scientifique of France, and the University of Hawaii. This project made use of the HyperLeda and NED data bases. Part of this work is based on data obtained from the ESO/ST-ECF Science Archive Facility.

REFERENCES

Arnold R., de Zeeuw P. T., Hunter C., 1994, MNRAS, 271, 924
Bacon R. et al., 1995, A&AS, 113, 347
Bacon R. et al., 2001, MNRAS, 326, 23
Balcells M., 1991, A&A, 249, L9
Bender R., 1988a, A&A, 202, L5
Bender R., 1988b, A&A, 193, L7
Bender R., Doebereiner S., Moellenhoff C., 1988, A&AS, 74, 385
Bender R., Surma P., Doebereiner S., Moellenhoff C., Madejsky R., 1989, A&A, 217, 35
Bender R., Saglia R. P., Gerhard O. E., 1994, MNRAS, 269, 785
Bendo G. J., Barnes J. E., 2000, MNRAS, 316, 315
Bertola F., Capaccioli M., 1975, ApJ, 200, 439
Binney J., 1978, MNRAS, 183, 501
Binney J., 1980, MNRAS, 190, 873
Binney J., 2005, MNRAS, 363, 937
Binney J., Tremaine S., 2008, Galactic Dynamics, 2nd edn. Princeton Univ. Press, Princeton, NJ
Bureau M., Athanassoula E., 2005, ApJ, 626, 159
Cappellari M., 2002, MNRAS, 333, 400
Cappellari M., Copin Y., 2003, MNRAS, 342, 345
Cappellari M. et al., 2006, MNRAS, 366, 1126 (Paper IV)
Cappellari M. et al., 2007, MNRAS, 379, 418 (Paper X)
Chung A., Bureau M., 2004, AJ, 127, 3192
Ciotti L., Lanzoni B., 1997, A&A, 321, 724
Corsini E. M., Wegner G., Saglia R. P., Thomas J., Bender R., Thomas D., 2008, ApJS, 175, 462
Davies R. L., Efstathiou G., Fall S. M., Illingworth G., Schechter P. L., 1983, ApJ, 266, 41
de Zeeuw P. T., 1985, MNRAS, 216, 273
de Zeeuw P. T. et al., 2002, MNRAS, 329, 513 (Paper II)
Djorgovski S., 1983, JA&A, 4, 271
Emsellem E., Monnet G., Bacon R., 1994, A&A, 285, 723
Emsellem E. et al., 2004, MNRAS, 352, 721 (Paper III)
Emsellem E. et al., 2007, MNRAS, 379, 401 (Paper IX)
Falcón-Barroso J. et al., 2006, MNRAS, 369, 529
Franx M., Illingworth G., de Zeeuw P. T., 1991, ApJ, 383, 112
Gebhardt K. et al., 2003, ApJ, 583, 92
Gerhard O., Kronawitter A., Saglia R. P., Bender R., 2001, AJ, 121, 1936
Gerhard O. E., 1993, MNRAS, 265, 213
González-García A. C., Balcells M., Olshevsky V. S., 2006, MNRAS, 372, L78
Halliday C., Davies R. L., Kuntschner H., Birkinshaw M., Bender R., Saglia R. P., Baggley G., 2001, MNRAS, 326, 473
Hau G. K. T., Forbes D. A., 2006, MNRAS, 371, 633
Hernquist L., 1990, ApJ, 356, 359
Hubble E. P., 1936, Realm of the Nebulae. Yale Univ. Press
Illingworth G., 1977, ApJ, 218, L43
Jedrzejewski R. I., 1987, MNRAS, 226, 747
Jesseit R., Naab T., Burkert A., 2005, MNRAS, 360, 1185
Jesseit R., Naab T., Peletier R. F., Burkert A., 2007, MNRAS, 376, 997
Koprolin W., Zeilinger W. W., 2000, A&AS, 145, 71
Kormendy J., 1982, Morphology and Dynamics of Galaxies, Proceedings of the Twelfth Advanced cource, Saas-Fee, Observatoire de Geneve, p. 113
Kormendy J., Bender R., 1996, ApJ, 464, L119+
Kormendy J., Illingworth G., 1982, ApJ, 256, 460
Krajnović D., Cappellari M., de Zeeuw P. T., Copin Y., 2006, MNRAS, 366, 787
Kronawitter A., Saglia R. P., Gerhard O., Bender R., 2000, A&AS, 144, 53
Kuntschner H. et al., 2006, MNRAS, 369, 497
Lauer T. R., 1985, ApJS, 57, 473
McDermid R. M. et al., 2006, MNRAS, 373, 906 (Paper VIII)
Merritt D., Quinlan G. D., 1998, ApJ, 498, 625
Naab T., Burkert A., 2001, ApJ, 555, L91
Naab T., Jesseit R., Burkert A., 2006, MNRAS, 372, 839
Peletier R. F., Davies R. L., Illingworth G. D., Davis L. E., Cawson M., 1990, AJ, 100, 1091
Qian E. E., de Zeeuw P. T., van der Marel R. P., Hunter C., 1995, MNRAS, 274, 602
Rix H., White S. D. M., 1990, ApJ, 362, 52
Rix H.-W., Franx M., Fisher D., Illingworth G., 1992, ApJ, 400, L5
Rix H.-W., Carollo C. M., Freeman K., 1999, ApJ, 513, L25
Rubin V. C., Graham J. A., Kenney J. D. P., 1992, ApJ, 394, L9
Ryden B. S., Terndrup D. M., Pogge R. W., Lauer T. R., 1999, ApJ, 517, 650
Saglia R. P., Bertschinger E., Baggley G., Burstein D., Colless M., Davies R. L., McMahan R. K. Jr, Wegner G., 1997, ApJS, 109, 79

Sandage A., 1961, The Hubble Atlas of Galaxies. Carnegie Institution, Washington
Sandage A., Bedke J., 1994, The Carnegie Atlas of Galaxies. Carnegie Institution of Washington with The Flintridge Foundation, Washington, DC
Sandage A., Sandage M., Kristian J., 1975, Galaxies and the Universe. Chicago, University of Chicago Press, p. 839
Schweizer F., 1979, ApJ, 233, 23
Schweizer F., 1981, AJ, 86, 662
Statler T. S., 1991, AJ, 102, 882
Tremaine S. D., 1987, in de Zeeuw P. T., ed., IAU Symp. Vol. 127, Structure and Dynamics of Elliptical Galaxies. Reidel, Dordrecht, p. 367
van den Bergh S., 1990, ApJ, 348, 57
van den Bosch R. C. E., van de Ven G., Verolme E. K., Cappellari M., de Zeeuw P. T., 2008, MNRAS, 385, 647
van der Kruit P. C., Allen R. J., 1978, ARA&A, 16, 103
van der Marel R. P., 1991, MNRAS, 253, 710
van der Marel R. P., 1994, MNRAS, 270, 271
van der Marel R. P., Franx M., 1993, ApJ, 407, 525
van der Marel R. P., Rix H. W., Carter D., Franx M., White S. D. M., de Zeeuw T., 1994, MNRAS, 268, 521
Wegner G., Corsini E. M., Saglia R. P., Bender R., Merkl D., Thomas D., Thomas J., Mehlert D., 2002, A&A, 395, 753

APPENDIX A: INFLUENCE OF SEEING ON THE SHAPE OF THE VELOCITY MAPS

The effects of seeing on galaxy images in the regime of non-adaptive optic assisted observations are now well understood (Saglia et al. 1997). They are specifically important in the nuclear regions where the instrumental effects and the atmospheric seeing redistribute photons sufficiently enough to change the intrinsic ellipticity or position angle and mask structures like concentrated stellar nuclei or double nuclei (Schweizer 1979, 1981; Djorgovski 1983; Lauer 1985). Specifically, luminosity profiles are affected more by the seeing when the ellipticity is low, while the ellipticity profiles are affected more when the ellipticity is high (Peletier et al. 1990). In general, effects of seeing can be detected to quite large radii.

It is natural to expect the redistribution of photons due to the seeing will also influence the two-dimensional shape (maps) of the higher moments of the LOSVD. Specifically, for the first moment, the mean velocity, the obvious effect of larger seeing is a less steep rise of the velocity in the centre. Additionally, one can expect an increased axial ratio (rounder map), or in other words, a more open spider diagram in the central regions. Except for these qualitative expectations there are no quantitative estimates of the influence of seeing on the shape of velocity maps. Observations of the SAURON sample were taken under a variety of atmospheric conditions, so before analysing the velocity maps, we tested the effects of different PSFs.

We constructed a number of model velocity maps using a Hernquist (1990) potential which reasonably well approximates the density of real early-type galaxies. Each model map was constructed from the Hernquist circular velocity profile, projected at a certain inclination to imitate different axial ratios seen in the sample ($q_{\rm kin}$), and weighted by the given Hernquist surface brightness profiles. All models have the same scalelength $r_0 = 10$ arcsec. The inclinations ranged from 20° to 75°, where 0° and 90° are face-on and edge-on viewing angles, respectively. This corresponds to velocity maps with axial ratios $q_{\rm kin}$ in the range of 0.94–0.26. Although in the SAURON sample there are near to edge-on galaxies, their velocity maps do not resemble the limiting case of edge-on discs ($q_{\rm kin} = 0$), being considerably less flat. The above range in axial ratios were used to match the values observed in the SAURON sample. Maps were then convolved with a Gaussian kernel of different full width at half-maximum (FWHM), accounting also for the square pixels (Qian et al. 1995) in such a way as to make the model maps similar to observations, especially in the central regions which remain unbinned. The range of FWHM was also matched to the measured seeing range of SAURON observations (Paper III). Fig. A1 shows an example of model maps for axial ratio of 0.5 and seeing FWHMs of 1, 2 and 3 arcsec.

We ran kinemetry on the convolved model velocity maps and extracted the same parameters as for the observed velocity maps: $\rm PA_{kin}$, $q_{\rm kin}$, k_1 and k_5/k_1 harmonics. The results can be seen in Fig. A2 and they suggest the following.

(i) Determination of the position angle is not influenced by the seeing.

(ii) The influence of the seeing on the determined axial ratio is larger on maps with intrinsically smaller axial ratio. Also, the bigger the seeing is, the rounder (larger axial ratio) is the observed map.

(iii) The influence of the seeing on the rotation curve (k_1 term) is larger on maps with intrinsically smaller axial ratios, where the bigger is the seeing, the lower is the maximum velocity. The position of maximum velocity is also pushed towards larger radii.

(iv) The influence of the seeing on the higher terms (k_5/k_1) is negligible in most cases, except for intrinsically very flat maps, but even there the signal is of the order of 1 per cent or less and is not detectable with the current accuracy.

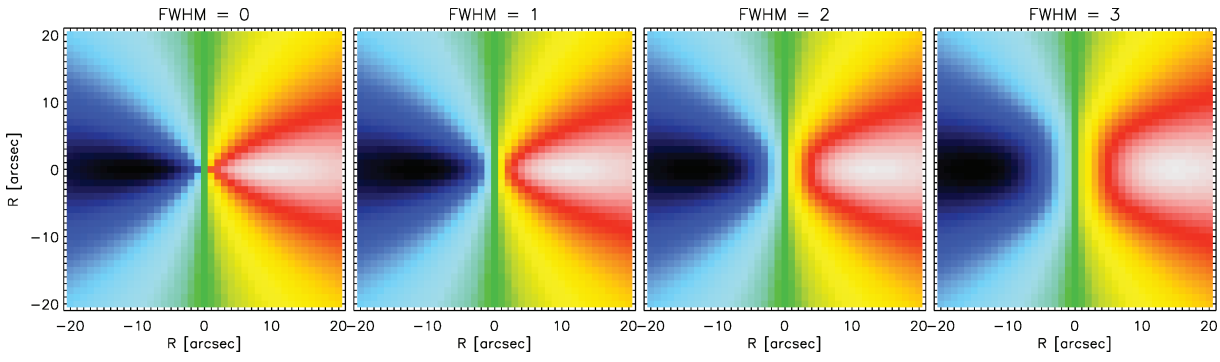

Figure A1. An example of model velocity maps for a given inclination and convolved with different seeing kernels. From left- to right-hand side: A model velocity map at axial ratio of 0.5 prior to convolution with seeing. Model velocity maps convolved with 1, 2 and 3 arcsec FWHM seeing, respectively. Note the change in the isovelocity contours in the centre with the increasing seeing.

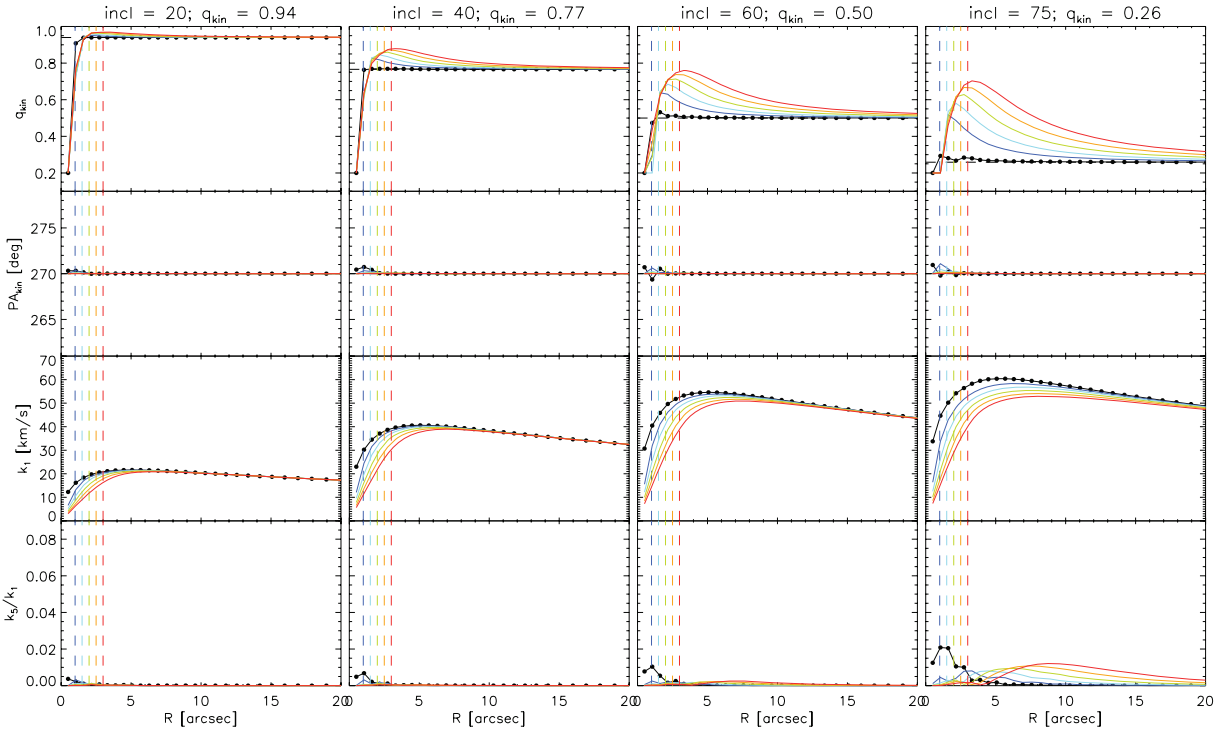

Figure A2. Kinemetric analysis of seeing convolved model velocity maps. From left- to right-hand side: Kinemetry coefficients from maps with axial ratios of 0.94, 0.77, 0.5 and 0.26. From top to bottom: Kinemetric coefficients: position angle, axial ratio, k_1 and k_5/k_1 harmonics. Colours correspond to values extracted from maps convolved to different seeing. Black: unconvolved model map. Blue: model map convolved with FWHM of 1 arcsec. Light blue: model map convolved with FWHM of 1.5 arcsec. Green: model map convolved with FWHM of 2 arcsec. Yellow: model map convolved with FWHM of 2.5 arcsec. Orange: model map convolved with FWHM of 3 arcsec. Vertical lines show the radial extent of the seeing at FWHM. Note that the incorrect determination of axial ratio at the innermost radius is an artefact of poor sampling.

As expected, the seeing influences the axial ratio of velocity maps (or, in other words, the opening of the isovelocity contours), and the steepness of the rotation curve, both in the maximum values and the positions of these maxima.

The largest effect is for maps with small axial ratio (large opening angles), which can be understood as the consequence of the convolution, similar as in the case of photometry and high ellipticity. In terms of changing of the intrinsic values, it is the axial ratio that is the most affected by seeing. At an intrinsic flattening of 0.77, a bad seeing of 2.5 arcsec, will increase the flattening by 0.1. This effect rises to surprising 0.5 difference in measured flattening for an intrinsic flattening of 0.26. This effect is milder for the maximum rotation velocity, where only for velocity maps with the smallest axial ratios and strongest seeings the difference between the intrinsic and seeing convolved values exceeds 10 km s^{-1}. Another effect of seeing on the velocity maps is the change of position of the maximum axial ratio and the maximum rotational velocity with increasing seeing. In both cases the trend is clear: larger seeing FWHM causes displacement of the maximum (q_{kin} or k_1) towards larger radii.

In summary, seeing can strongly influence the appearance of the velocity maps, both in the shape, value and extent of the features. This is important for interpreting the structures on the maps and, especially, when looking for kinematic subcomponents.

APPENDIX B: KINEMETRIC PROFILES

In this section we present the results of kinemetric analysis of SAURON velocity maps (Fig. B1).

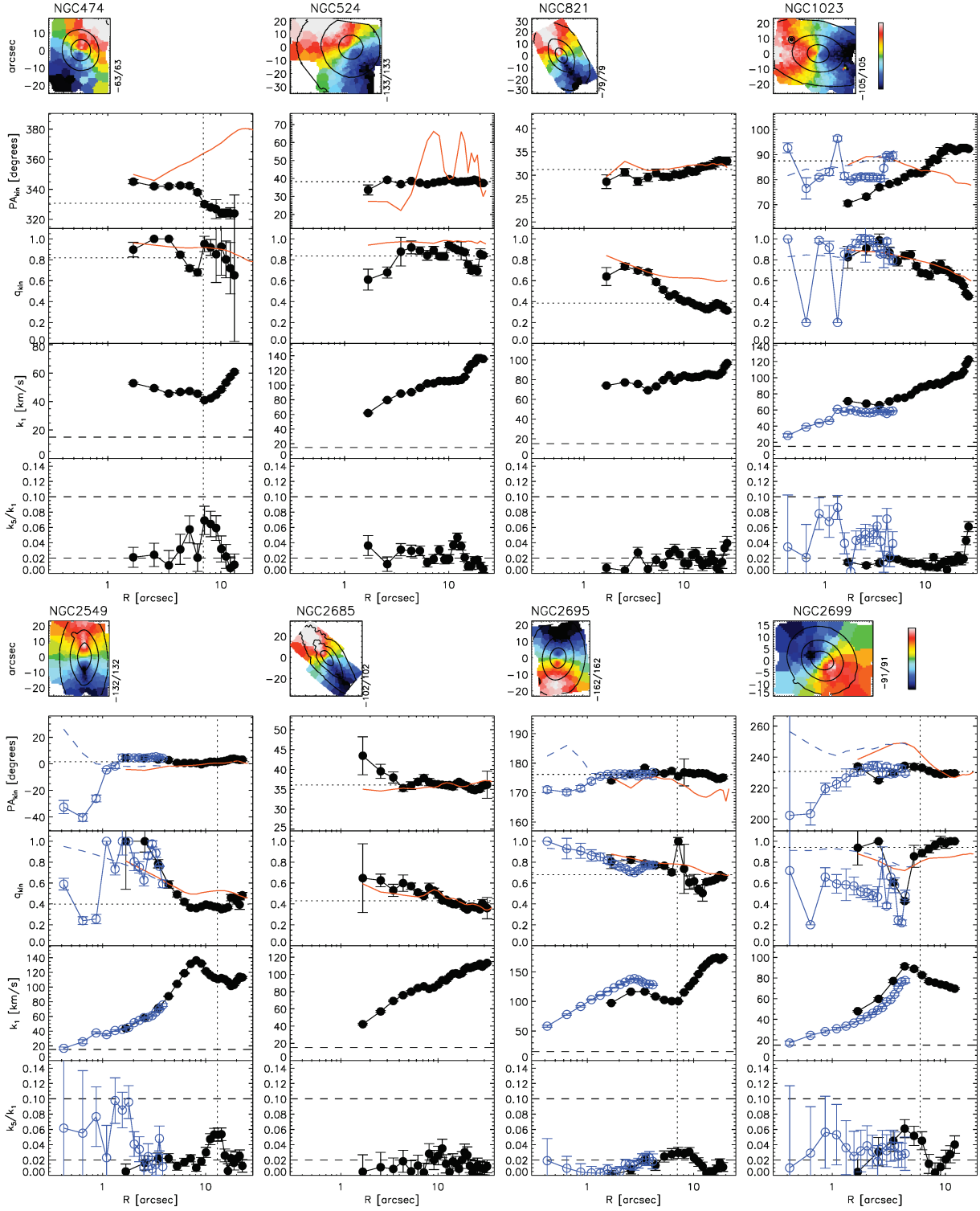

Figure B1. Kinemetric profiles of 48 early-type galaxies. The panels show (from top to bottom) SAURON stellar mean velocity map, and extracted kinemetric properties: position angle, axial ratio, k_1 and k_5/k_1 coefficients. Solid black symbols are SAURON data, open blue circles are OASIS data. Solid light blue and green symbols are results of kinemetry on circles for OASIS and SAURON data, respectively. Red line shows photometric $\mathrm{PA_{phot}}$ and q_{phot} from the SAURON reconstructed images. Dashed blue line shows photometric $\mathrm{PA_{phot}}$ and $1-\epsilon$ from the OASIS reconstructed images. Dashed horizontal lines on k_1 and k_5/k_1 panels show the limiting cases: $k_1 = 15\,\mathrm{km\,s^{-1}}$ limit of detectable rotation, $k_5/k_1 = 0.02$ limit of detectable deviation from the assumed cosine function in kinemetry, $k_5/k_1 = 0.1$ limit for doing kinemetry on circles. These limits are data dependant (for more details see Section 4). Dashed lines on $\mathrm{PA_{kin}}$ and q_{kin} panels show luminosity-weighted average values of the radial profiles. In the case of global $\langle q_{\mathrm{kin}} \rangle$ innermost 5 arcsec are excluded due to the seeing effects.

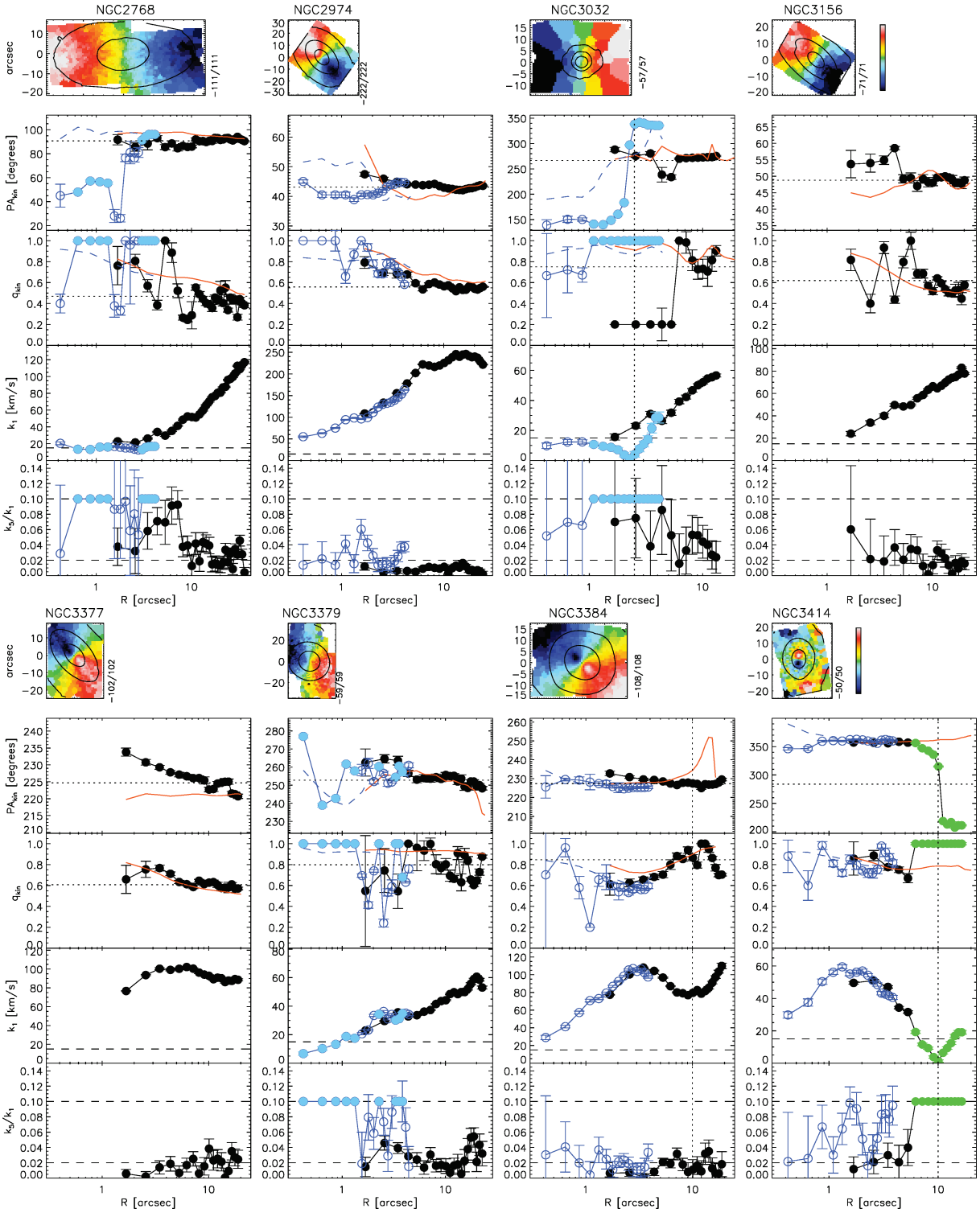

Figure B1 – *continued*

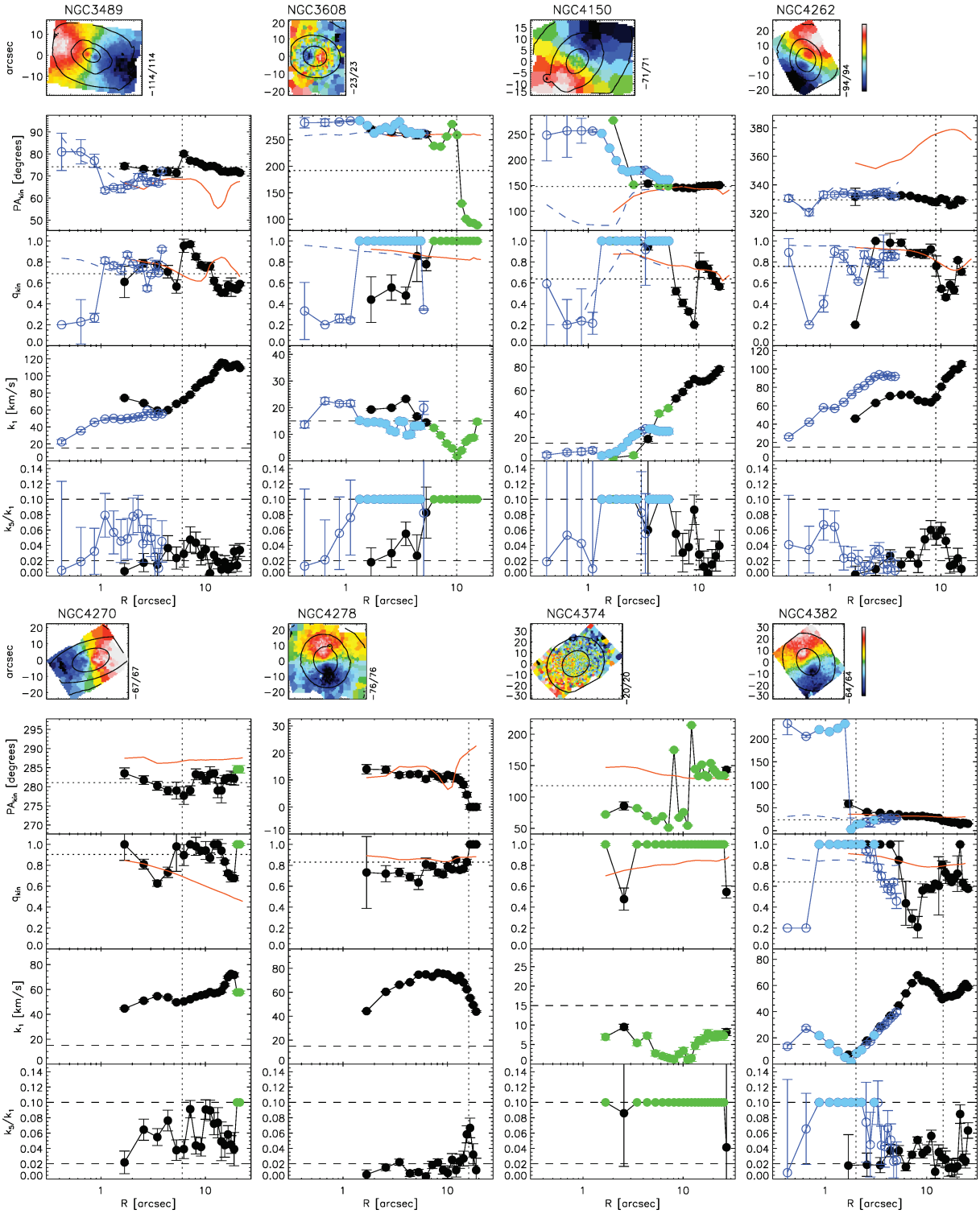

Figure B1 – *continued*

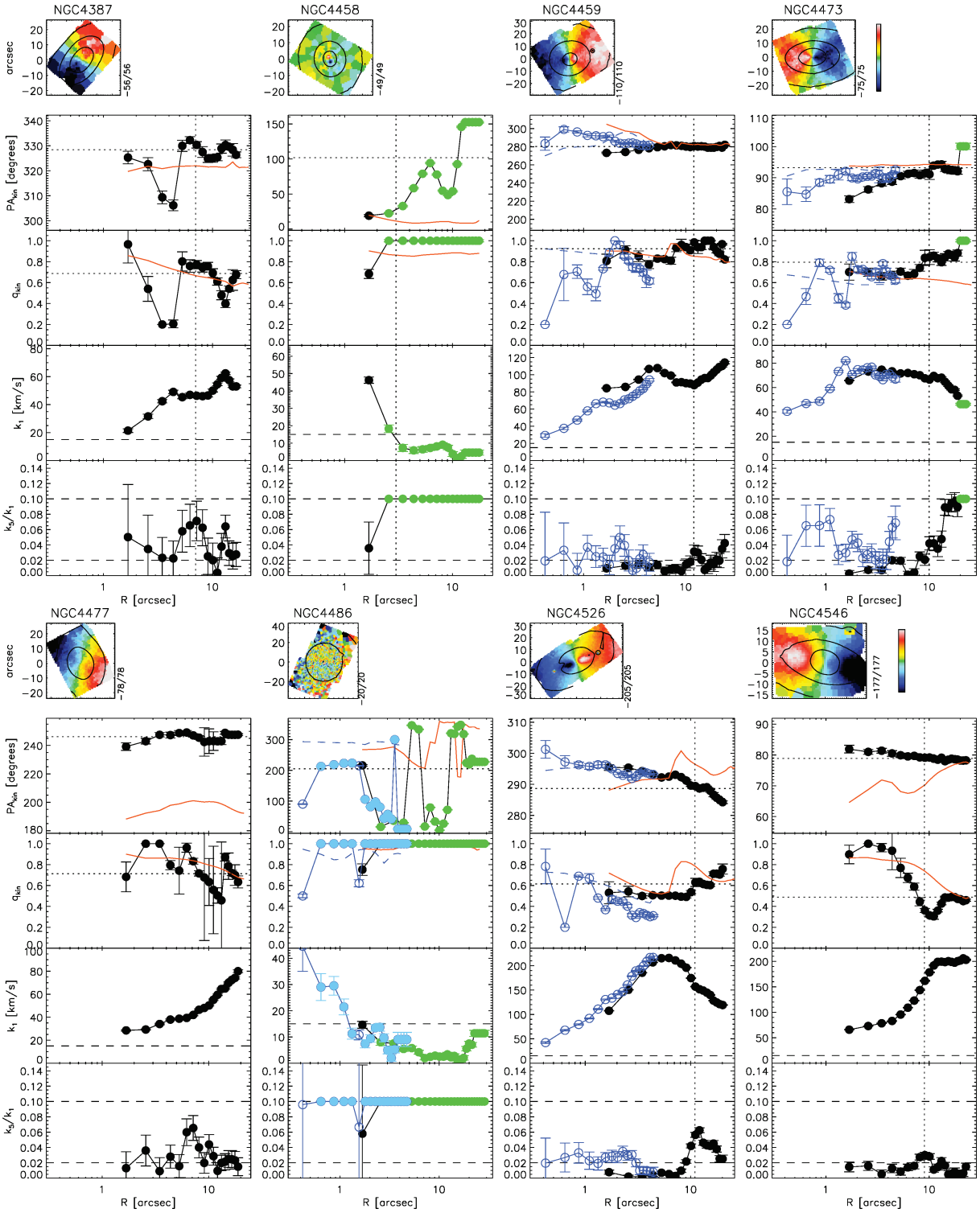

Figure B1 – *continued*

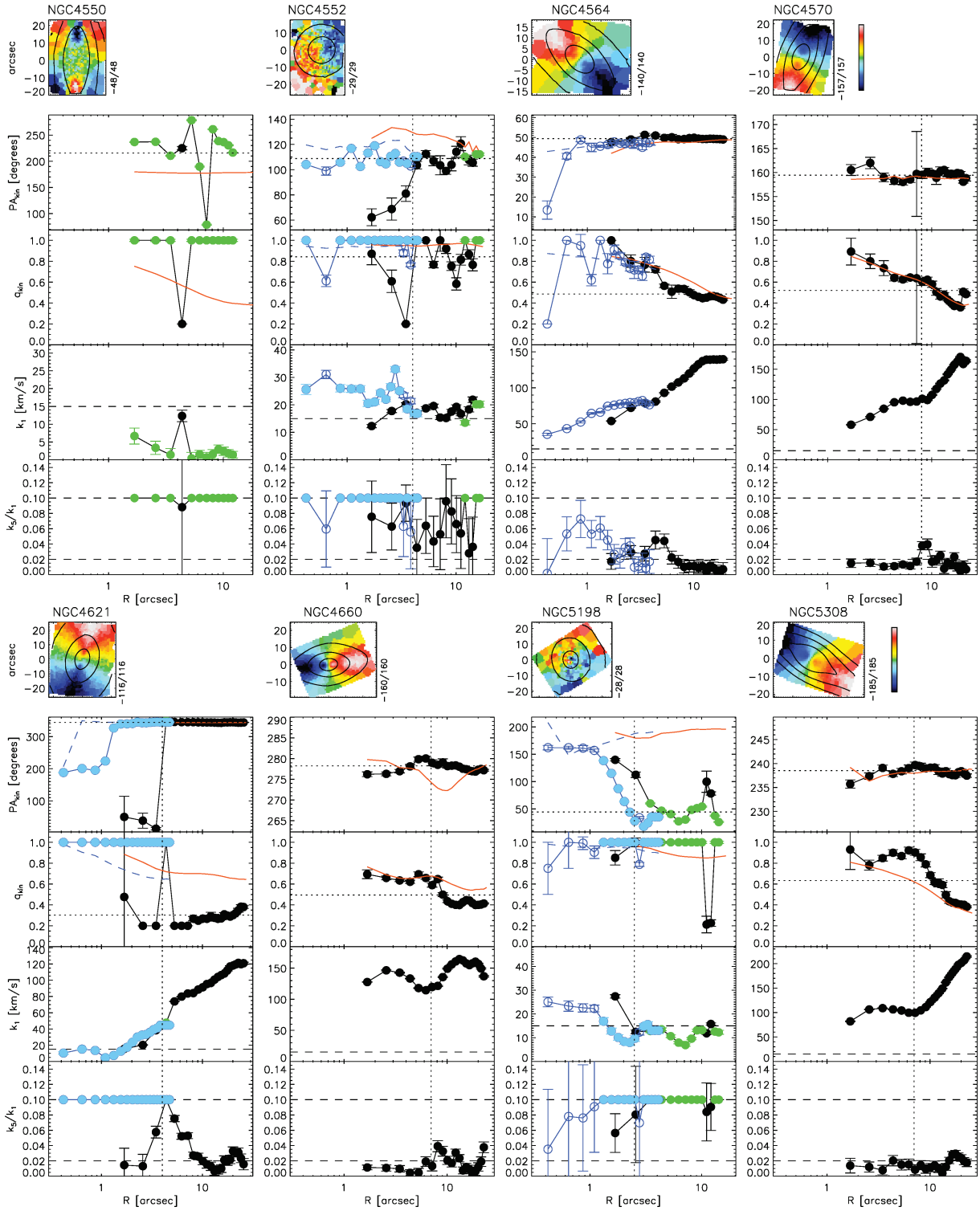

Figure B1 – *continued*

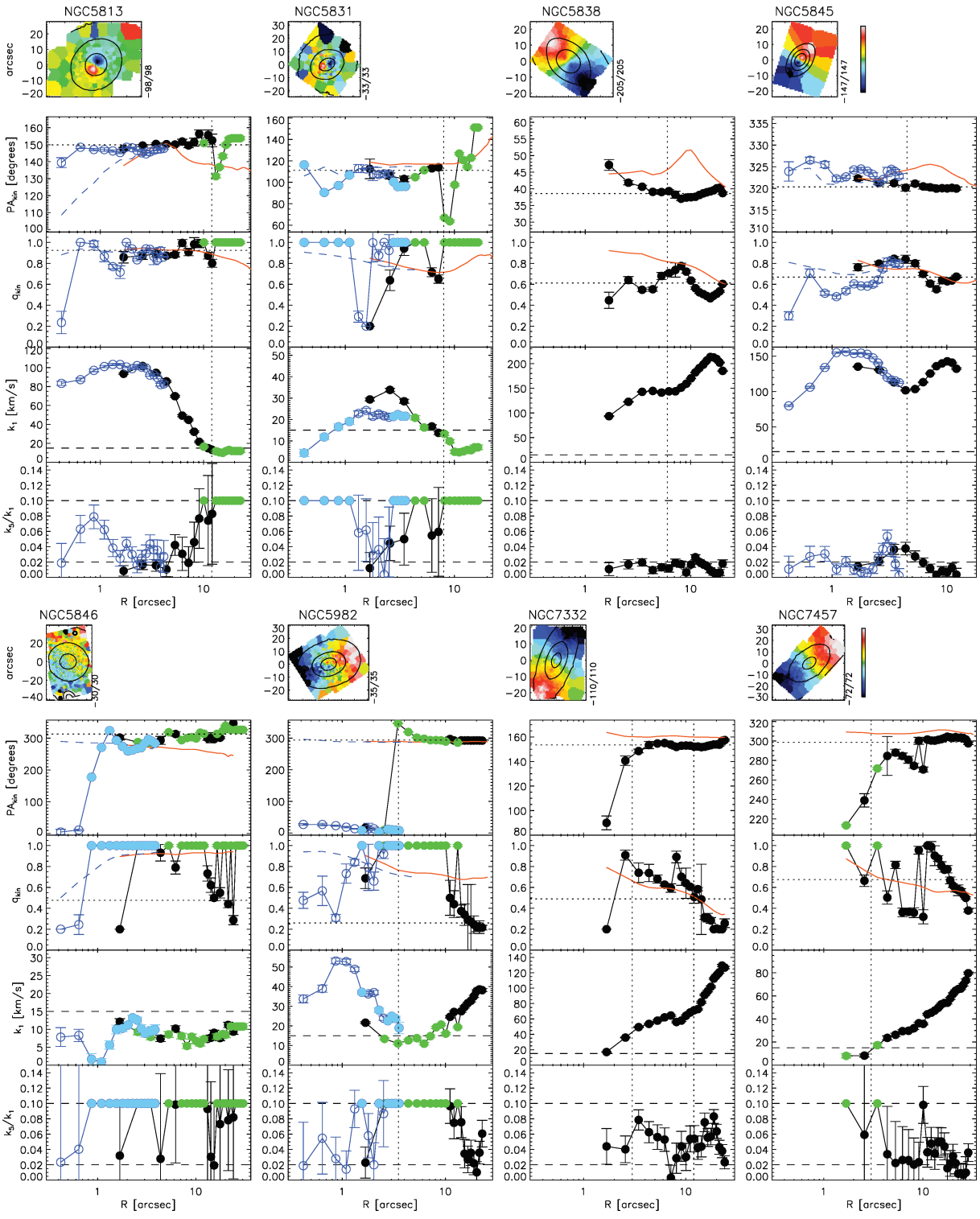

Figure B1 – *continued*

This paper has been typeset from a TEX/LATEX file prepared by the author.